Mon. Not. R. Astron. Soc. **269,** 928–946 (1994)

Parsec-scale radio cores in early-type galaxies

O. B. Slee,[1] Elaine M. Sadler,[2,3] J. E. Reynolds[1] and R. D. Ekers[1]

[1] *Australia Telescope National Facility, CSIRO, PO Box 76, Epping, NSW 2121, Australia*
[2] *Anglo-Australian Observatory, PO Box 296, Epping, NSW 2121, Australia*
[3] *School of Physics, University of Sydney, NSW 2006, Australia*

Accepted 1994 March 18. Received 1994 March 16; in original form 1993 October 1

ABSTRACT

We find compact (< 0.03 arcsec) radio-continuum cores in about 70 per cent of radio-emitting elliptical and S0 galaxies over a wide range in total radio power (10^{21}–10^{26} W Hz^{-1} at 5 GHz). The cores usually have a flat or rising spectrum between 2.3 and 8.4 GHz, with a median spectral index of +0.3. Even at low luminosities, the radio emission from most elliptical galaxies appears to be powered by a parsec-scale 'engine' like those in classical radio galaxies and quasars. The core and total radio power are related ($P_{\rm core} \propto P_{\rm total}^{0.7}$ on average), and the parsec-scale cores of radio galaxies are typically one hundred times more powerful than those in 'normal' giant elliptical galaxies.

Key words: galaxies: active – galaxies: elliptical and lenticular, cD – galaxies: nuclei – radio continuum: galaxies.

1 INTRODUCTION

Powerful double-lobed radio galaxies appear to be powered by parsec-scale 'engines' in their nuclei. Classical radio galaxies in which the radio emission extends far beyond the optical galaxy are rare, but smaller and less luminous radio-continuum sources are commonly seen in the nuclei of nearby elliptical and S0 galaxies (e.g. Sadler, Jenkins & Kotanyi 1989; Wrobel & Heeschen 1991). Are these sources scaled-down versions of the engines that power radio galaxies, or does the radio emission arise from a different mechanism such as a small starburst? A powerful way of discriminating non-thermal engines from star-forming regions is by long-baseline radio observations (Norris et al. 1990). Such observations can detect sources with the high brightness temperatures characteristic of quasar cores (> 10^5 K), but are insensitive to the more extended radio emission produced by starbursts.

In a preliminary study, Slee et al. (1990) used the 275-km Parkes–Tidbinbilla interferometer (PTI) at 2.3 GHz to observe a complete sample of 34 nearby E and S0 galaxies already known to be weak radio sources. They detected compact (< 0.1 arcsec) cores in 70 per cent of the sample, suggesting that low-luminosity sources (10^{20}–10^{22} W Hz^{-1}) in these galaxies arise from the same process that powers radio galaxies and quasars. We have now extended this work to a larger sample of early-type galaxies spanning a wide range in total radio power, and have measured radio spectral indices for most of the detected cores. Our aim is to see how the core properties vary with total radio power, and with other galaxy properties.

Throughout this paper, we use $H_0 = 75$ km s^{-1} Mpc^{-1} and $q_0 = 0.5$. For other values of H_0, the quantities we derive can be converted as follows (for $h = H_0/100$ km s^{-1} Mpc^{-1}):

Absolute magnitude: $M_B(h) = M_B(0.75) + 0.625 + 5\log(h)$;

Radio power: $\log P(h) = \log P(0.75) - 0.25 - 2\log(h)$;

Space density: $\log \Phi(h) = \log \Phi(0.75) - 0.375 - 3\log(h)$.

2 OBSERVATIONS AND REDUCTION

2.1 Sample selection

Our goal was to study core luminosities and spectra over a wide range of total radio power, and so we observed two different galaxy samples. Since the galaxies in both our samples are less powerful radio emitters than the 3C sources which form the basis of most very long-baseline interferometry (VLBI) studies, we refer to them as the low- and medium-power samples.

2.1.1 *The low-power sample (A)*

At the low-luminosity end (10^{20}–10^{23} W Hz^{-1} at 5 GHz) we used the sample of E/S0 galaxies south of declination −32° studied by Sadler (1984a, b, c). This covers 1.27 sr, is 90 per cent complete at $B_T = 13.8$ mag, and has been surveyed with the Parkes 64-m telescope to a limiting flux density of 25 mJy at 2.7 GHz. Galaxies north of −45° in this sample have also been mapped at 5 GHz at the Very Large Array (VLA)

(Sadler et al. 1989), with a limiting flux density of 0.8 mJy. Sample A comprises the 42 galaxies in Sadler's complete sample with 5-GHz flux densities above 8 mJy, a further 23 elliptical galaxies north of $-32°$ declination known to be radio sources from other surveys (Ekers & Ekers 1973; Disney & Wall 1977; Ulvestad & Wilson 1984; Birkinshaw & Davies 1985; Impey, Wynn-Williams & Becklin 1986), and two S0/a galaxies south of $-32°$, NGC 612 and IC 5063, which are strong radio sources but were excluded from the Sadler sample on classification grounds.

2.1.2 *The medium-power sample (B)*

To study more powerful radio galaxies (typically 10^{22}–10^{26} W Hz^{-1} at 5 GHz), we observed the 91 galaxies mapped by Ekers et al. (1989) at the VLA at 1.5 and 5 GHz. These sources have flux densities above 200 mJy in the Parkes 2.7-GHz survey and have been identified with galaxies brighter than 17th magnitude. This sample covers 1.78 sr of sky and includes eight members of the low-power sample as well as several nearby spiral galaxies. A V/V_{max} test (Schmidt 1968) shows that the medium-power sample is complete for elliptical galaxies above combined radio and optical limits of 200 mJy (at 2.7 GHz) and $m_b = 16.0$ mag (i.e. somewhat brighter than the cut-off magnitude $m = 17.0$ listed by Ekers et al. 1989).

Table 1 gives the log of our PTI and Australia Telescope (AT) observations and, for completeness, includes the results already published by Slee et al. (1990). Fig. 1 shows a histogram of the total radio power at 5 GHz for galaxies in the two samples. For much of the analysis that follows, we merged the samples to give a combined list of 140 E and S0 galaxies (the 'combined sample').

It is often difficult to classify an individual galaxy unambiguously as E or S0 (e.g. van den Bergh 1989), particularly when it is distant or contains dust, but most of the galaxies observed here are likely to be ellipticals rather than true S0s. The radio-continuum sources in S0 galaxies are weaker on average than those in ellipticals and the detection rate in surveys of optically selected samples is correspondingly lower (Hummel & Kotanyi 1982; Sadler et al. 1989). Only 20 (14 per cent) of the 140 E and S0 galaxies in the merged sample are classified as S0 and some of these (e.g. NGC 1947) are actually dust-lane ellipticals, and so the true fraction of S0s may be even lower.

2.2 PTI observations

The Parkes–Tidbinbilla interferometer (PTI) links the 64-m Parkes radio telescope in real time with either the 70-m or a 34-m antenna at the NASA Deep Space tracking station at Tidbinbilla, giving a 275-km SSE–NNW baseline (Norris et al. 1988). The main observing frequencies used in this programme were 2.295 and 8.41 GHz, giving fringe spacings of 90 and 27 milliarcsec (mas) respectively. We also had one observing session at 12.2 GHz with a fringe spacing of 19 mas, but the poorer phase stability and ten-fold reduction in sensitivity at this frequency meant that the data were of low quality. Many of the PTI detections were later observed at 4.73 GHz with the five-element compact array of the AT, at a resolution of ~ 5 arcsec.

The PTI observing sessions were usually limited to 12–16 h because of other commitments of NASA's Deep Space Network 70- and 34-m telescopes, but three of the 8.4-GHz

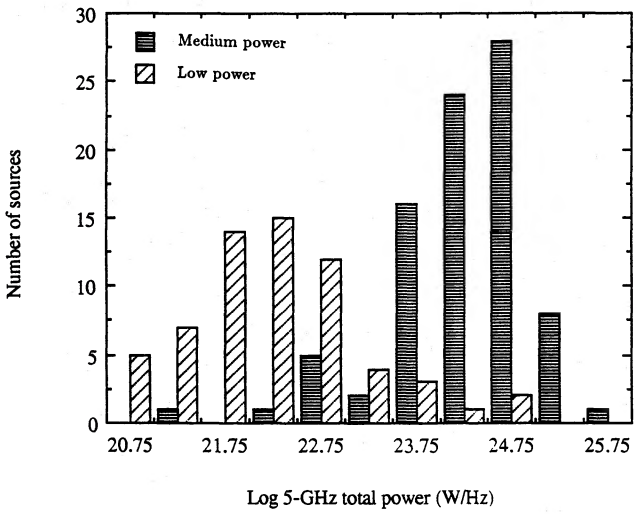

Figure 1. Histogram of total 5-GHz radio power for elliptical and S0 galaxies in samples A (low power) and B (medium power).

Table 1. Log of observing sessions.

Session Number	Observing Date	Frequency GHz	Antennas m	Bandwidth MHz	RMS Noise mJy	No. Observed A	No. Observed B
1	Mar-88	2.3	70, 64	10	0.8	38	6
2	Jul-88	2.3	70, 64	10	0.5	17	4
3	Nov-88	8.4	34, 64	10	1.8	5	4
4	Nov-88	8.4	70, 64	10	1.2	28	8
5	Apr-89	8.4	34, 64	5	1.6	17	91
6	May-89	8.4	34, 64	5	1.7	6	9
7	Nov-89	2.3	34, 64	10	1.3	2	3
8	Dec-89	2.3	34, 64	10	2.6	6	28
9	Jul-90	2.3	70, 64	10	0.6	3	20
10	Jul-90	12.2	70, 64	5	20	5	4
11	Mar-91	2.3	34, 64	10	0.8	3	8
12	Mar-91	2.3	70, 64	10	0.5	6	17
13	Jul-91	2.3	70, 64	10	0.5	4	4
14	May-90	4.7	5x22, AT	128	1.0	7	58
15	Sep-90	4.7	5x22, AT	128	1.0	25	39

sessions extended over two to four days (in contrast to the single days allocated at 2.3 GHz), so the total observing times for the two frequencies were similar. We used right-hand circularly polarized feeds on both antennas at 2.3 and 8.4 GHz, and linearly polarized antennas at 12.2 GHz. The use of linear polarization is acceptable when both telescopes are alt–az mounted, the parallactic angles at both sites are the same to within one or two degrees, and the source polarization is low (as is the case for most core sources).

2.2.1 *Calibration and reductions*

Each PTI observing period began with an observation of a strong compact source with accurately known coordinates to calibrate the interferometer delay and fringe frequency. No further adjustment of these was required during the 10–16 h observing sessions.

Individual source observations were 512 s in length at 2.3 and 8.4 GHz, and 256 s at 12.2 GHz, and were analysed by Fourier transforming the complex correlation coefficients (recorded every 2 s) over time to produce a function in offset fringe frequency. A strong compact source at the nominal observing position produces a narrow centrally located peak in this domain (see e.g. fig. 1 of Slee et al. 1990). This procedure allows coherent integration of the 2-s data points while solving for the source fringe frequency, which may be offset by errors in the assumed coordinates or drifts in the reference oscillators at the two antennas.

For all but one of the sessions we had to use a rubidium oscillator at Parkes (see Table 1), with some resulting decorrelation at the higher frequency. The effect of decorrelation is seen in the fringe frequency response as a broadening of the source peak with a corresponding reduction in amplitude (by as much as 20–30 per cent at 8.4 GHz). To compensate, source fluxes were estimated from the integrated area under the peak, rather than from the peak amplitude itself, a procedure estimated to incur errors of no more than 10 per cent in source flux.

Flux calibration of the individual source observations was done in the usual way. We used 16 calibrators, all of which are strong sources in the list of Preston et al. (1985) and unresolved with the PTI (R. Duncan et al. 1993, unpublished AT calibrator list). The total flux of each calibrator was determined from single-dish measurements against the primary flux calibrator, Hydra A, which was assumed to have flux densities of 27.5 and 8.4 Jy at 2.3 and 8.4 GHz respectively (Baars et al. 1977) with small corrections for the finite angular extent of the source. Conveniently placed calibrators were observed with the PTI every 3 h or so throughout the observing sessions.

The PTI flux calibrators are unresolved flat-spectrum sources, and may be variable. Table 2 lists the total flux density measurements of our calibrators at 8.4 GHz. We see variations of up to 10 per cent in the flux density of some calibrators over the three years of our observing programme (compared to a scatter of 3–5 per cent for calibrators observed several times in the same session), so it is important to measure the calibrator flux densities in each session when they are used for PTI calibration.

2.2.2 *Error estimates*

Several galaxies in our programme were observed more than once with the PTI, either in the same or in different observing sessions, and we can use the results to estimate the uncertainty in our measured flux densities. The main sources of error for an unresolved source are system noise, imperfectly known antenna gain and pointing corrections, variations in sky transparency and phase instability. Most of these effects are larger at 8.4 than at 2.3 GHz. The standard deviation of the observed 8.4-GHz fluxes is typically 6–9 per cent for unresolved sources observed several times in the same session and 10–20 per cent for the few sources observed in three or more separate sessions. In the latter case, intrinsic variations in the core flux may contribute to the scatter, and there is a further source of uncertainty in determining the system parameters for each session, especially at the Tidbinbilla end where three different antennas were used.

If a source is partly resolved by the PTI, the observed flux will also change systematically as the source moves across the sky, because of changes in the position angle and length of the projected baseline. For the few sources where we observed this effect (we will show later that most of the sources in the combined sample are unresolved), the change in flux with hour angle was <25 per cent.

Table 2. Calibrator flux densities at 8.4 GHz. Error in a measurement is 3–5 per cent.

Calibrator Name	Measured Flux Densities (Jy) in Sessions : Nov-86	Mar-87	Nov-88	Feb-89	Apr-89	Jun-89	Sep-89	May-90	Mean (Jy)
0008-264			0.52	0.43					0.48
0048-097			1.12	1.54		1.03			1.23
0237-233	2.56	2.72				2.20			2.49
0414-189			0.65	0.68		0.52			0.62
0434-188			1.01	1.03		0.90			0.98
0537-441			4.70			4.65			4.67
0637-752	6.78	8.37				6.40			7.18
1124-186			2.02					1.77	1.90
1222+037			0.92						0.92
1327-311			0.56						0.56
1502+036					0.56				0.56
1511-210					0.51				0.51
1610-771		2.51				3.15			2.83
1921-293			7.43	6.81		7.96			7.40
2008-159			1.35			1.17	1.28	1.28	1.27
2047+039			0.52						0.52

It seems reasonable therefore to adopt an uncertainty of 20 per cent for individual fluxes measured in a single run with the PTI. For objects observed more than once, the error should be somewhat less.

2.2.3 *The effects of position errors*

The delay compensation and phase of the PTI are adjusted to be correct at the position adopted for the radio core. If the adopted radio position is incorrect, the fast Fourier transform (FFT) response will appear at a non-zero fringe offset and will be reduced by an amount (due to incorrect delay compensation) which depends on how much the source's position is offset in the direction perpendicular to the projected baseline. The 'delay beamwidth' to full width at half-maximum (FWHM) in this direction is 54 arcsec, and so errors of 4–5 arcsec in the core positions (typical of published galaxy positions) will not reduce the measured PTI amplitude significantly. In practice, we saw little evidence for position errors since the measured fringe offset frequency rarely exceeded 5 MHz. The narrow 'delay beamwidth', in conjunction with antenna primary beamwidths of only a few arcmin, ensured that confusion problems were negligible.

Fig. 2 shows the interferometer response for the spiral galaxy ESO 253 − G3 (observed in a separate programme), one of the few galaxies where a confusing source is present. Here, the spiral galaxy itself is seen at fringe frequency zero with a peak flux of 19 mJy, while the strong source PKS 0524 − 460 is detected at an offset frequency of about + 50 MHz. PKS 0524 − 460 has also been observed as a VLBI target by Preston et al. (1985), and is 196 arcsec from ESO 253 − G3.

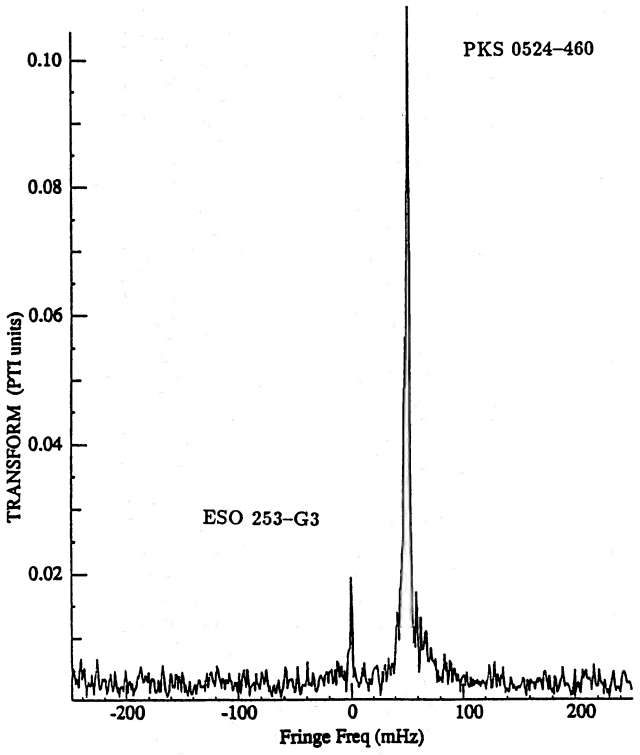

Figure 2. Interferometer response for spiral galaxy ESO 250 − G3, showing the confusing source PKS 0524 − 460.

2.3 Australia Telescope observations

We also used the compact array of the AT at 4.7 GHz to observe most of the galaxies detected with the PTI. This was done for several reasons:

(i) to obtain an extra point on the core spectrum between the PTI frequencies of 2.3 and 8.4 GHz;

(ii) to measure more accurate core positions for sources south of −45° which have not been mapped with the VLA; and

(iii) to check for long-term flux variability in the sources mapped at the VLA at 4.9 GHz during 1979–84 by Ekers et al. (1989) and Sadler et al. (1989).

We used the five-element compact array (the sixth antenna, which gives a 6-km baseline, having not yet been commissioned at the time of our observations) in its highest-resolution configuration, with a maximum baseline of 3 km and a minimum fringe spacing of 5 arcsec. Each source was observed twice, 5–7 h apart, with a total integration time of 20 min. We interleaved observations of the programme sources with hourly observations of strong unresolved calibrators with accurately known positions, whose flux densities were measured against the primary flux calibrator PKS 1934 − 638.

The u–v data were checked and calibrated with the AIPS software in the usual way, and the two observations of each source were then merged to make dirty maps, although the short-baseline visibilities were discarded if they showed a rise in amplitude above those of the longer baseline visibilities, a procedure intended to eliminate the large-scale structure in the image. If a source was present near the phase centre (the phase centres were displaced 30 arcsec to the south of the nominal core position), the map was appropriately cleaned. If the source was stronger than 20 mJy, the map was self-calibrated with a point-source model, which usually improved the dynamic range.

In a few cases we were unable to detect a core with the compact array even though there was unambiguous evidence for its presence from the PTI (e.g. PKS 0336 − 35 in Table 4). This appears to be because we did not observe our chosen AT calibrators frequently enough to calibrate the u–v data effectively. (The five-element compact array has relatively few baselines and little redundancy, and at the time of these observations the local oscillator phase stabilization was not yet implemented.) Once the phase calibration was good enough to detect a source, however, the application of self-calibration dramatically improved its visibility.

Flux density errors for the AT measurements are difficult to assess. We do not have multiple observations of any sources, and so cannot check the consistency of our error estimates as we did for the PTI data. The lowest contour on our maps, presumably due to noise and uncleaned side-lobes of the target sources (and in some cases other sources in the AT primary beam), varied between 0.6 and 6.5 mJy with a well-defined mean of ~1 mJy. Thus for unresolved sources we might expect an error of ~10 per cent in the measured flux of a 10-mJy core. The error due to noise would be less for stronger cores, but if there is strong extended emission the side-lobe levels will also be higher because of poor u–v coverage and less effective cleaning. The side-lobes of confusing sources outside the field may also raise the noise level.

A realistic error for the AT fluxes therefore appears to be ~20 per cent.

2.4 Core fluxes

Tables 3 and 4 list core and total flux densities for the low- and medium-power samples. As discussed above, errors are typically 20 per cent for both PTI and AT measurements. We also derived an estimated 5-GHz PTI flux for each galaxy by interpolating linearly between the observed 2.3- and 8.4-GHz fluxes (where a galaxy was observed at only one frequency, we used the median index of +0.28 for the interpolation). This allows us to compare the PTI data with observations on larger scales, most of which have been made at 5 GHz.

Tables 3 and 4 also list 5-GHz AT and VLA fluxes for core components (on scales of 1–5 arcsec). The AT flux densities are from our own measurements, and the VLA fluxes are from the literature (sources are indicated in the notes to each table). The total 5-GHz fluxes listed in each table are also from the literature and are Parkes single-dish measurements unless indicated otherwise in the notes.

2.5 Core positions from the Australia Telescope observations

Sadler et al. (1989) give accurate VLA positions in their table 1 for most of the galaxies in our low-luminosity sample. Here, in Table 5, we list the AT positions (accurate to ±1 arcsec in both coordinates) for the remaining galaxies. We also

Table 3. Core and total flux densities for sample A (low-power ellipticals).

— Galaxy —					— Flux density (mJy) —							
B1950	Name	Type	B mag	Dist. Mpc	PTI 2.3 GHz	PTI 8.4 GHz	Interp 5 GHz	AT 4.8 GHz	VLA 4.9 GHz	Total 5 GHz	Sessions	Ref
(1)	(2)	(3)	(4)	(5)	(6)	(7)	(8)	(9)	(10)	(11)	(12)	(13)
0007–572	149–G19◇	E/S0	14.0	125	<4		<5			197	1	
0106–805	013–G12◇	S0	13.6	64.6	<4		<5			87	1	
0123–016	NGC 547	E	13.2	72.8	68	124	97			2250	2,3	DW
0131–367	NGC 612*	S0	13.9	119	22	31	27	33	28	2200	5,8,11,14,15	
0136–079	NGC 636	E	12.4	24.9	<3		<5			6	2	IWB
0136–427	NGC 641◇	E	13.1	82.5	8	17	13	10	10	101	1,4,15	
0153+053	NGC 741	E	12.2	76.3	13	9	10			220	4,11	EE
0238–084	NGC 1052	E/S0	11.4	20.5	708	2898	1643		1270	1218	2,3	DW
0303–158	NGC 1209	E	12.4	35.3	15	20	18	12	9	12	2,4,5,15	IWB
0320–374	NGC 1316*◇	S0	9.4	21.7	<3	<9	<6		26	65800	1,5,13	DW
0336–355	NGC 1399*◇	E	10.6	17.4	15	20	18	<2	10	342	1,3,4,5,6,11,14,15	DW
0337–187	NGC 1407	E	10.7	22.9	<3		<5			44	2	DW
0343–041	NGC 1453	E	12.6	51.4	21	18	19			18	2,4,5	DW
0415–559	NGC 1553◇	S0	10.3	13.5	<4		<5			<30	1	
0428+005	NGC 1587	E	12.7	51.0	7	10	9			80	2,4,5,6	EE
0429–051	NGC 1600	E	11.9	63.1	<3	<5	<5			22	2,4	DW
0526–638	NGC 1947◇	S0	11.7	13.0	<4		<5			18	1	
0549–074	NGC 2110	E	14.0	30.4	32	49	41		106	175	6,8	UW
0714–352	367–G08◇	S0	13.4	35.3	<4		<5		<1	<30	1	
0727–622	IC 2200A◇	S0	13.9	39.5	<4		<5			<30	1	
0835–549	NGC 2640◇	S0	12.4	10.0	23	42	33	42		29	1,3,4,15	
0843–336	NGC 2663◇	E	11.9	24.5	116	168	144	183	160	1039	1,4,10,15	
0931+103	NGC 2911	S0	12.5	39.9	50	38	43		163	150	6,8	EE
0941–210	NGC 2986	E	11.7	28.4	<4		<5			33	2	DW
0956–266	NGC 3078	E	12.1	29.7	111	155	136		113	130	2,5	DW
0958–314	NGC 3100*	E	12.0	32.0	173	125	143	217	590	510	5,8,14,15	
1024–396	NGC 3250◇	E	12.2	33.9	<4		<5		<1	21	1	
1026–353	NGC 3258◇	E	12.5	33.7	<4		<5		4	52	1	
1027–350	NGC 3268◇	E	12.5	33.5	27	15	19	15	23	28	1,4,15	
1029–459	263–G48◇	S0	12.5	34.6	<4		<5		2	20	1	
1034–272	NGC 3309	E	12.6	50.5	<3		<5		<3	14	2	DW
1107–372	NGC 3557*◇	E	11.4	35.6	13	27	20	24	10	299	1,4,5,8,9,12,14,15	
1127–361	NGC 3706◇	S0	12.4	40.6	<2		<5		8	19	13	
1222–394	NGC 4373◇	E	11.9	42.1	4		5		13	12	12	
1232+124	NGC 4550	E/S0	12.6	13.7		<7	<6		<1	39	6	W
1240+029	NGC 4636	E/S0	10.4	11.0	<2		<5			45	3,12	F87
1246–410	NGC 4696◇	S0	11.3	34.8	25	14	18	131	55	1393	1,4,15	
1250–151	NGC 4756	E	13.4	55.5	<2	<16	<5			98	2,3	DW
1250–102	NGC 4760	E	12.3	56.6	52	38	43			460	2,4	DW
1301–302	NGC 4936	E	11.9	40.9	51	33	39			87	2,5	DW

Table 3 – *continued*

— Galaxy —					— Flux density (mJy) —							
B1950	Name	Type	B mag	Dist. Mpc	PTI 2.3 GHz	PTI 8.4 GHz	Interp 5 GHz	AT 4.8 GHz	VLA 4.9 GHz	Total 5 GHz	Sessions	Ref
(1)	(2)	(3)	(4)	(5)	(6)	(7)	(8)	(9)	(10)	(11)	(12)	(13)
1310–420	323–G93◇	S0	13.4	43.0	14	20	17	24	21	33	1,4,15	
1312–161	NGC 5044	E	11.7	33.1	19	31	25			30	2,4,5	DW
1316–123	NGC 5077	E	12.4	35.7	201	337	274			167	2,4,5,10	DW
1318–434	NGC 5090◇	E	12.6	42.6	409	770	597	662	268	1632	1,4,5,10,15	
1322–427	NGC 5128◇	E	7.8	4.3	3500		6456	6139	6984	126000	1,9,10,15	DW
1323–336	NGC 5140◇	S0	12.8	49.0	23	27	25	34	29	43	1,5,15	
1333–336	IC 4296*◇	E	11.6	45.8	181	422	300	222	214	1604	1,5,10,12 14	
1339–479	NGC 5266◇	S0	12.0	37.8	<6		<8			<30	7	
1400–337	NGC 5419*◇	S0	11.9	54.6	8	<6	8	49	15	390	1,5,9,12,14,15	
1503+017	NGC 5846	S0	11.1	22.3	7		8		5	8	12	F89
1646–607	137–G45◇	E	13.3	42.6	12		14	9		33	1,15	
1902–689	NGC 6730◇	E	13.1	55.3	39		44	35		67	1,15	
1909–563	NGC 6758◇	E	12.7	43.1	<4		<5			28	1	
1940–517	232–G21◇	S0	14.7	52.3	<4		<5			33	1	
2003–485	NGC 6861◇	E	12.1	37.0	5	<5	6	5		20	1,4,15	
2006–485	NGC 6868◇	E	11.7	36.3	72	79	76	65		124	1,4,15	
2015–412	IC 4991◇	S0	12.3	75.5	<4		<5		1	20	1	
2045–381	NGC 6958◇	E	12.3	36.1	13	16	15	10	18	27	1,4,15	
2048–572	IC 5063	S0/a	12.9	43.8	140	10	29			516	6,13	s
2054–488	NGC 6987◇	E/S0	13.4	70.4	23	25	24	29		57	1,4,15	
2100–492	NGC 7002◇	E	13.5	99.5	17	32	25	24		48	1,4,15	
2103–427	286–G50◇	E	13.7	35.0	<4		<5		<1	<30	1	
2115–487	NGC 7049◇	S0	11.7	28.3	16	14	15	19		35	1,4,15	
2137–427	NGC 7097◇	E	12.6	31.7	29		34		18	18	13	
2206–474	NGC 7213◇	S0	11.0	23.1	176	334	258	234		228	1,4,7,15	
2208–689	NGC 7216◇	E	13.5	44.3	30	36	33	38		46	1,4,15	
2254–367	IC 1459*◇	E	11.0	22.5	835	446	574	1181	1016	1073	1,4,5,14	

Columns are as follows.
(1) Identifier based on B1950.0 position.
(2) Galaxy name. Galaxies marked ◇ belong to the complete sample south of Dec. −35° studied by Sadler (1984a, b, c), and those marked * also belong to the medium-power sample of Ekers et al. (1989).
(3) Galaxy type.
(4) Apparent magnitude B_T, from de Vaucouleurs et al. (1992).
(5) Distance in Mpc, calculated for $H_0 = 75$ km s^{-1} Mpc^{-1} and $q_0 = 0.5$.
(6), (7) Flux densities measured in this study with the PTI at 2.3 and 8.4 GHz.
(8) Interpolated PTI 5-GHz flux density (see text).
(9) Core flux density measured with the Australia Telescope (this study – see text for details).
(10) Core flux density measured with the VLA, from Sadler et al. (1989) or Ekers et al. (1989), except for NGC 1209 (Cordey 1986) and NGC 2110 (Ulvestad & Wilson 1983).
(11) Total 5-GHz flux density, from Sadler (1984c), Ekers et al. (1989) or published values from the sources listed in column 13.
(12) PTI observing sessions (see Table 1).
(13) References for total 5-GHz flux: DW, Disney & Wall (1977); EE, Ekers & Ekers (1973); F87, Fabbiano et al. (1987); F89, Fabbiano, Gioia & Trinchieri (1989); IWB, Impey, Wynn-Williams & Becklin (1986); s, Sadler (1983, unpublished Parkes measurements); UW, Ulvestad & Wilson (1983); w, Whiteoak (1970).
Notes on individual sources.
NGC 1052. VLA core flux from Wrobel & Heeschen (1984). The compact source structure is discussed by Jones et al. (1984).
NGC 2110. VLA core flux from UW.
NGC 2911. VLA core flux from Wrobel & Heeschen (1984).
NGC 3078. VLA core flux from Wrobel & Heeschen (1984).
NGC 3309. VLA core limit from Lindblad, Jörsäter & Sandqvist (1985).
NGC 4550. Also detected by Haynes & Sramek (1975), but not by Impey et al. (1986). VLA core limit from Wrobel & Heeschen (1991).
NGC 5419. Ekers et al. list a total 5-GHz flux density of 390 mJy for this galaxy, quoting Wall & Schilizzi (1979). This includes the contribution from extended emission to the east of the galaxy, and thus is higher than the value of 150 mJy measured by Sadler (1984c) at Parkes. Goss et al. (1987) discuss the radio structure in detail.
NGC 5846. VLA core flux density from Wrobel & Heeschen (1991).

Table 4. Core and total flux densities for sample B (medium-power radio galaxies).

Name	Type	B mag	Dist. Mpc	Flux density (mJy) PTI 2.3 GHz	PTI 8.4 GHz	Interp. 5 GHz	AT 4.8 GHz	VLA 4.9 GHz	Total 5 GHz	Sessions
(1)	(2)	(3).	(4)	(5)	(6)	(7)	(8)	(9)	(10)	(11)
0005–199	E	16.5	470	8	16	12	20	14	250	5,11,14
0007–325	E	14.4	101	131	283	207	292	230	350	5,8,14
0013–240	S	16.9	258	125	60	81	149	190	230	5,8,14
0013–316	E	16.5	412		<6	<5		5	130	5
0023–333	E	14.6	206	8	18	13	12	10	410	5,6,11,14
0038–210	E	17.4	362		<5	<5		160	330	5
0045–255	Sc	7.0	2.8		<4	<5		130	2080	5
0048–233	E	17.6	459		<6	<5		<10	200	5
0131–367*	S0	13.9	119	22	31	27	33	28	2200	5,8,11,14,15
0155–212	E	17.8	648	34	31	32	50	35	220	5,8,14,15
0229–208	E	16.0	360	56	111	84	113	93	470	5,8,14,15
0244–304	Sb	10.6	16.4	<5	<6	<6		<3	150	5,7
0247–207	E	15.4	348	14	29	22	14	23	300	5,11,14,15
0257–398	E	15.3	270		<4	<4		<4	430	5
0307–305	E	16.0	270		<6	<5		3	390	5
0312–343	E	15.6	267	22	<6	25		25	220	5,13
0320–374*	S0	9.4	21.7	<3	<9	<6		26	65800	1,5,13
0331–363	Sb	11.2	21.6	<5	<5	<5		<1	210	5,6,7
0332–391	E	15.3	250	12	16	14	16	13	420	5,11,14,15
0336–355*	E	10.6	17.4	15	20	18	<2	10	342	1,3,4,5,6,11,14,15
0344–345	E	16.0	215	49	82	67	275	40	930	3,4,5,8,14
0344–291	DB	17.4	528	17	18	18	35	33	250	5,11,12,14.,15
0349–278	E	16.1	261	9	25	17	8	16	2210	2,3,4,5,14,15
0434–225	E	14.6	273		<7	<6		9	390	5
0446–206	E	16.4	289		<6	<5		9	220	5
0449–175	E	14.4	126	5	13	9	7	10	310	5,6,12,14,15
0452–190	E	14.5	149	22	26	24	11	25	190	5,12,14,15
0453–206	E	14.4	137	26	29	28		40	1780	5,12,14,15
0505–375	S	11.2	8.0	6	<6	6		15	220	5,7,13
0511–305	E	16.3	233	6	16	11	5	10	750	2,5,14,15
0521–365	N	16.0	222	1298	3007	2125	2160	1400	9230	5,8,14
0523–327	D	15.4	303	11	18	15	<3	15	370	5,12,14,15
0533–377	E	16.7	386	11	18	15	21	13	160	5,12,14
0546–315	E	17.7	594		<5	<5		5	140	5
0546–329	E	14.5	148	23	36	30	<5	32	220	5,8,14,15
0548–322	BL	15.5	276	31	42	37	71	70	230	5,8,14,15
0548–317	E	14.5	130		<7	<6		<6	430	5
0618–371	DB	15.2	130	17	22	20	<5	15	1280	5,12,14,15
0625–354	E	16.0	221	410	559	493	862	600	2090	5,8,14
0634–205	E	16.5	224	10	14	12	<5	12	3550	2,3,4,5,6,12,14,15
0712–349	E	15.9	174	26	38	33	42	25	170	5,8,14,15
0718–340	E	15.4	114	25	37	32	19	30	950	5,8,14,15
0940–304	E	14.5	150	23	42	33	60	47	190	5,8,14
0958–314*	E	12.0	32.0	173	125	142	217	590	510	5,8,14,15
1002–320	E	17.4	351	<1	<6	<5		<5	230	5,8
1043–290	E	15.4	229	39	56	48	56	55	280	5,8,14,15
1053–282	E	15.5	237	99	185	144		115	890	5,8,14,15
1056–360	E	16.0	278	49	71	61	52	50	510	5,8,14,15
1107–372*	E	11.4	35.6	13	27	20	24	10	299	1,4,5,8,9,12,14,15
1123–351	E	14.5	128	44	57	52	36	70	790	5,8,14
1142–341	D	15.6	272	<2	<5	<5		15	110	5,9
1144–327	D	15.3	242	<2	<7	<5		10	190	5,9
1159–185	Irr	11.3	23.2		<8	<7		<5	240	5
1228–335	D	15.4	222	15	22	19	1"	13	210	5,6,9,12,14,15
1251–289	E	14.4	231	12	13	13	82	<10	240	5,6,9,14
1254–300	D	15.2	216		<6	<5		<5	370	5
1257–253	E	16.0	258	14	23	19	13	16	270	5,9,12,14,15
1258–321	E	12.8	59.6	91	149	122	30	100	790	5,8,14,15
1306–241	S	15.5	53.6	148	44	72	228	210	220	5,8,14
1323–271	E	15.5	173	16	31	24	19	15	500	5,8,9,12,14,15

Table 4 – *continued*

Name	Type	B mag	Dist. Mpc	Flux density (mJy) PTI 2.3 GHz	PTI 8.4 GHz	Interp. 5 GHz	AT 4.8 GHz	VLA 4.9 GHz	Total 5 GHz	Sessions
(1)	(2)	(3)	(4)	(5)	(6)	(7)	(8)	(9)	(10)	(11)
1329–328	D	15.6	193	<10	<6	<7		<6	400	5,8
1333–336*	E	11.6	45.8	181	422	300	222	214	1604	1,5,10,12,14
1334–29	S	8.0	1.6		<7	<6		<4	760	5
1344–241	S0	14.4	75.9		<8	<7		<4	200	5
1354–251	E	15.4	150	7	<7	7		5	300	5,9
1400–337*	E	11.9	54.6	8	<6	8	49	15	390	1,5,9,12,14,15
1404–267	E	14.4	82.7	397	354	371	374	280	400	5,8,10,12,14
1413–364	E	17.5	301		<6	<5		<5	770	5
1514–241	BL	16.0	220	1346	1143	1221	1807	2800	1940	5,9,10,12,14
1521–300	E	15.3	81.1	158	292	228	272	160	400	5,9,10,12,14
1928–340	E	17.4	386		<5	<5		21	190	5
1929–397	E	15.3	295		<6	<5		14	990	5
2013–308	E	15.4	355	6	11	9	<5	10	280	5,6,9,14,15
2031–359	E	15.5	350	30	28	29		12	590	5,9,14,15
2040–267	E	14.6	152	12	26	19	57	32	910	5,9,14,15
2058–282	E	15.3	154	54	72	64	84	74	1960	5,9,14,15
2059–311	E	14.5	153	17	<7	17		18	200	5,13
2104–256	E	15.2	156	38	70	55	40	65	3970	5,9,14,15
2128–388	E	14.4	74.0	20	23	22	32	20	400	5,9,14,15
2158–380	E	14.6	133		<6	<5		<5	590	5
2206–237	E	17.6	346	205	32	68	1026	1100	980	2,4,5,6,8,14,15
2209–255	E	15.9	252	51	52	52	72	50	260	5,9,14,15
2225–308	E	15.8	220	14	37	25	67	30	340	5,9,14,15
2236–176	E	15.3	296		<7	<6		10	540	5
2236–364	D	15.2	227	29	45	38	57	8	310	5,9,14,15
2254–367*	S0	11.0	22.5	835	446	574	1181	1016	1073	1,4,5,14
2331–240	E	15.9	188	553	800	690	968	1100	1060	5,8,11,14
2333–327	E	14.6	208		<6	<5		12	130	5,14
2350–374	E	16.0	459		<6	<5		<4	210	5
2353–184	E	16.0	289		<6	<5		<10	310	5
2354–350	D	14.5	192		<7	<6		7	110	5

Columns are as follows.
(1) Object name. Galaxies marked * also belong to sample A (Table 3).
(2) Galaxy type.
(3) Apparent magnitude B_T, from Ekers et al. (1989) or Table 3 (for galaxies in common).
(4) Distance in Mpc, calculated for $H_0 = 75$ km s^{-1} Mpc^{-1} and $q_0 = 0.5$.
(5), (6) Flux densities measured in this study with the PTI at 2.3 and 8.4 GHz.
(7) Interpolated 5-GHz PTI flux density.
(8) Core flux density measured with the Australia Telescope (this study – see text for details).
(9) Core flux density measured with the VLA, from Ekers et al. (1989).
(10) Total 5-GHz flux density, from Ekers et al. (1989) or Sadler (1984c).
(11) PTI observing sessions (see Table 1).

measured the AT core positions of a further 10 galaxies with VLA positions measured by Sadler et al. (1989) and the two sets of measured positions agree to within 1 arcsec.

3 RESULTS

3.1 Detection rate

The overall detection rate for PTI cores in the merged sample of 140 E/S0 galaxies is 70 per cent, and this is roughly constant for radio powers between 10^{21} and 10^{26} W Hz^{-1} (see Fig. 3). At first sight this is remarkable, and implies that elliptical galaxies spanning a factor of 100 000 in radio power share the common property that their nuclei contain parsec-scale radio cores of high brightness temperature.

3.2 Spectral index distribution

We define the radio spectral index α between two frequencies ν_1 and ν_2 as

$$\alpha = \frac{\log(S_1/S_2)}{\log(\nu_1/\nu_2)},$$

where S_1 and S_2 are the measured flux densities at the two frequencies.

Fig. 4 shows a histogram of PTI spectral indices between 2.3 and 8.4 GHz for the low- and medium-power samples. The two distributions are similar, with a median value of $+0.28$ for the combined sample. This is closer to the median core spectral index of $+0.01$ for a small sample of core-

Table 5. AT positions of low-power cores south of −45° or not previously measured.

Galaxy Name	Core Flux at 5 GHz mJy	Core Position (1950) RA h m s	DEC ° ′ ″
NGC 1209	18	03 03 42.9	-15 48 15
NGC 2640	33	08 36 05.0	-54 56 51
NGC 5090	590	13 18 17.5	-43 26 34
NGC 5128	6456	13 22 31.6	-42 45 33
137-G45	14	16 46 35.3	-60 43 25
NGC 6730	44	19 02 13.1	-68 58 38
NGC 6861	6	20 03 42.2	-48 31 12
NGC 6868	75	20 06 16.4	-48 31 39
NGC 6987	24	20 54 41.9	-48 49 26
NGC 7002	24	21 00 17.0	-49 13 42
NGC 7049	15	21 15 37.0	-48 46 23
NGC 7213	254	22 06 08.4	-47 24 45
NGC 7216	33	22 08 43.1	-68 54 33

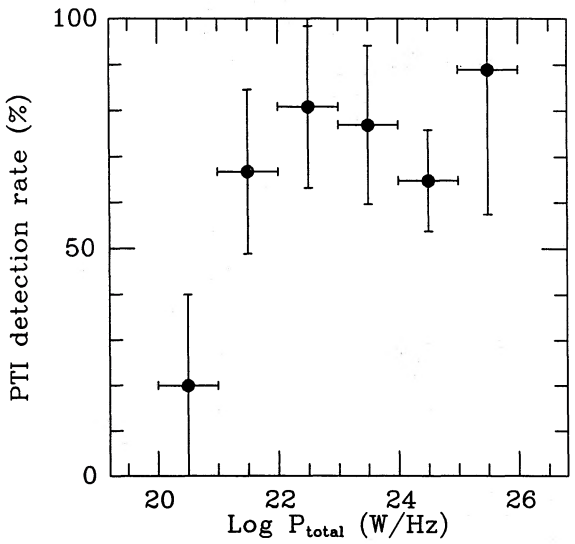

Figure 3. Detection of PTI cores as a function of total radio power at 5 GHz. Since only five galaxies with $P_{total} < 10^{21}$ W Hz^{-1} were observed, the low detection rate in the leftmost bin may not be significant.

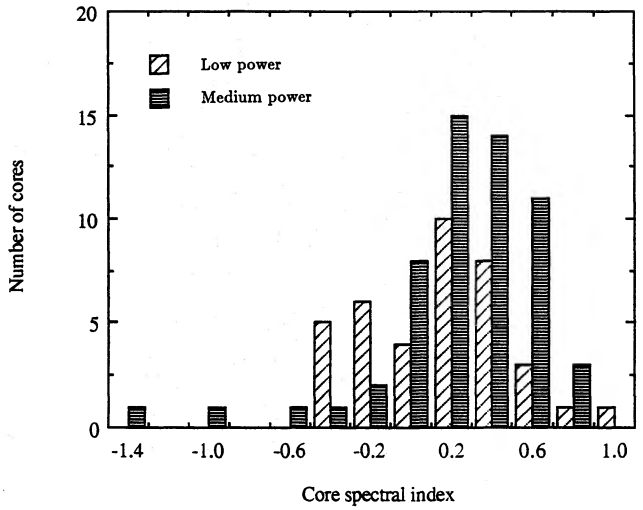

Figure 4. Histogram of PTI core spectral indices between 2.3 and 8.4 GHz for the two samples.

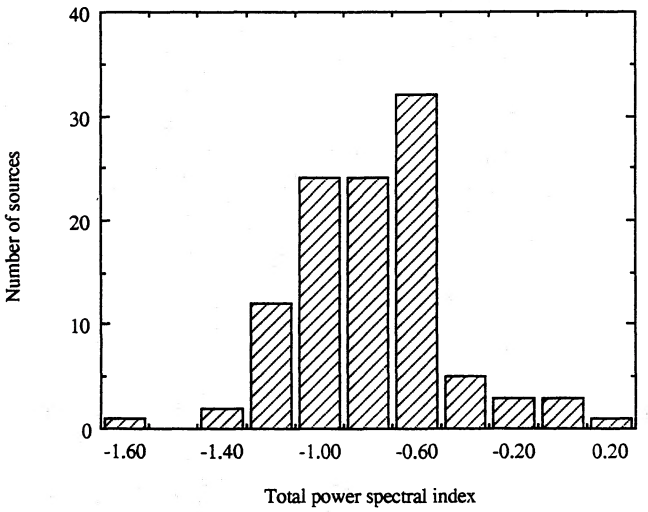

Figure 5. Histogram of whole source (total power) spectral indices for the medium-power sample. The median spectral index is −0.7, in contrast with the value of +0.3 for the cores in Fig. 4.

dominated quasars observed by O'Dea, Barvainis & Challis (1988) than to the values of −0.7 to −0.8 typically observed for the extended (kiloparsec-scale) emission from radio galaxies (see Fig. 5), and suggests that the parsec-scale radio cores in nearby elliptical galaxies are qualitatively similar to those in powerful radio galaxies and quasars.

Table 6 lists the nine sources observed at 12.2 GHz, along with the overall spectral index from 2.3 to 12.2 GHz and partial indices from 2.3–8.4 and 8.4–12.2 GHz. Although 0915−118 (Hydra A) is not one of our sample sources, it was observed frequently and so has an accurately determined core spectrum.

We examined the data for correlations between core spectral index and the following parameters: core power, total power, core-to-lobe ratio, *Einstein* X-ray luminosity and [N II] emission-line luminosity. No significant correlations were found, although very few of the galaxies have X-ray and [N II] measurements. We will discuss the relation between radio core properties and *IRAS* infrared fluxes in a later paper.

3.3 How many cores are partly resolved?

In galaxies with compact radio cores, how much of the radio emission in the central kiloparsec comes from the core itself? In other words, are most 'core sources' measured at arcsec resolution from AT or VLA maps dominated by a milliarcsec-scale component, or is there significant structure on scales of 0.1–5 arcsec (perhaps from a jet or star-forming region)? PKS 2206−237 in Table 4 is one example of a galaxy where the PTI flux is far lower than that measured with the VLA and the AT, suggesting that the core is partly resolved. NGC 1052 also has extended flux in the inner few arcseconds, but the nucleus itself is not resolved (Wrobel & Heeschen 1984).

Table 6. PTI core flux densities and spectral indices for sources observed at 12.2 GHz.

Galaxy Name		PTI Core Flux Densities			Spectral Indices		
PKS	Other	2.3 GHz mJy	8.4 GHz mJy	12.2 GHz mJy	2.3-12.2 GHz	2.3-8.4 GHz	8.4-12.2 GHz
0843-336	NGC 2663	116	168	160	0.22	0.29	-0.13
0915-118	Hydra A	175	267	392	0.44	0.33	1.03
1316-123	NGC 5077	201	337	240	0.18	0.40	-0.91
1318-434	NGC 5090	409	770	636	0.32	0.49	-0.51
1322-427	NGC 5128	3500	6561†	7721	0.46†	0.83†	0.18†
1333-337	IC 4296	181	422	322	0.42	0.65	-0.72
1404-267		397	354	259	-0.21	-0.09	-0.84
1514-241	AP Lib	1346	1143	1966	0.14	-0.13	1.45
1521-300		158	292	397	0.53	0.47	0.82

†No 8.4-GHz observation; average of 4.9-GHz AT and VLA measurements used for spectra.

We can estimate the fraction of core sources with extended structure on scales of 0.1 to 5 arcsec by considering the observed distribution of the ratio of core flux densities $S_{\rm PTI}/S_{\rm arcsec}$ at 5 GHz, where $S_{\rm arcsec}$ is the flux density at a few arcsec resolution measured with the VLA or the AT. This ratio should be 1.0 for a non-varying source that is unresolved by both the AT and the PTI. In practice, errors in PTI flux measurements, uncertainty in the shape of the core spectrum between 2.3 and 8.4 GHz (assumed linear for our interpolation of PTI fluxes to 5 GHz) and intrinsic core variability will scatter the measurements of this ratio about a mean $S_{\rm PTI}/S_{\rm arcsec}$. If some sources have arcsec-scale structure that is resolved out with the PTI but not with the VLA or the AT, there will be more galaxies with ratios below 1.0 than above.

Of the 100 galaxies in the combined sample with cores detected above 5 mJy with the VLA or the AT, 60 have $S_{\rm PTI}/S_{\rm arcsec} < 1.0$ and 40 have $S_{\rm PTI}/S_{\rm arcsec} > 1.0$. If the excess of objects with $S_{\rm PTI}/S_{\rm arcsec} < 1.0$ corresponds to galaxies where arcsec-scale flux is being resolved out, then there are roughly 10 such objects out of 100, suggesting that ~10 per cent of the cores in Tables 3 and 4 are partially resolved on arcsecond scales. Fig. 6 compares the PTI and VLA 5-GHz power.

On smaller angular size-scales, there are three pieces of evidence showing that most cores are unresolved.

(i) *The near equality of flux densities when a source is observed at different hour angles.* At 8.4 GHz, we observed 32 sources at two or more baseline position angles (in the same observing session) differing by 30°–75°. The median deviation from the mean flux density was 8.3 per cent, much of which is due to measurement error. Only five of the 32 cores showed deviations of 15 per cent or more and may be partly resolved, implying that at least 85 per cent of the cores we observed have angular sizes less than the PTI fringe spacing of 27 milliarcsec at 8.4 GHz.

(ii) *The predominance of positive spectral indices between 2.3 and 8.4 GHz.* The difference in angular resolution of the PTI at 2.3 and 8.4 GHz will affect the PTI spectral index if the cores have angular sizes close to the fringe separation of the PTI, with the cores being more resolved at 8.4 GHz. If this were the case, we would measure a lower flux density at the higher frequency. This is contrary to what we observe for most of the cores.

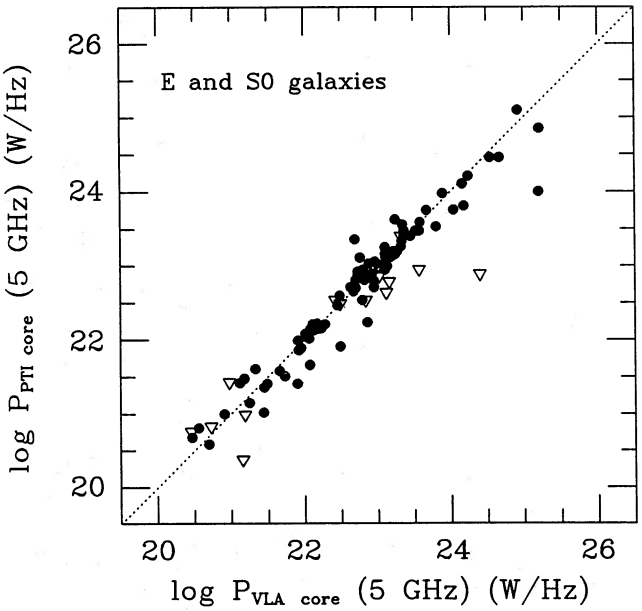

Figure 6. Comparison of the VLA (scale 1–5 arcsec) and PTI (scale 0.03–0.1 arcsec) core powers for E/S0 galaxies in the combined sample. Triangles denote sources where a core was detected with the VLA but not with the PTI.

(iii) *The similarity of the spectral index distributions for the low- and medium-power samples.* Galaxies in the medium-power sample are typically five times as distant as those in the low-power sample. If the cores of galaxies in the nearer sample were approaching resolution by the PTI while those in the more distant sample were unresolved, then we would expect the two samples to show different spectral index distributions. The similarity of the distributions in Fig. 4 again supports the idea that most of the cores are unresolved.

The radio cores of quasars have typical diameters of 0.5 mas at $z = 0.3$, and 1.5 mas at $z = 0.1$ (e.g. Ghisellini et al. 1992). If these are scaled to distances typical of our sample this gives sizes of roughly 12 mas at 50 Mpc and 30 mas at 20 Mpc. Since most of the cores we have observed are unresolved, they are probably no larger than a typical 'quasar' core.

1994MNRAS.269..928S

Table 7. Radio power and other derived quantities for sample A.

Name		Abs. mag	Log P (W/Hz) PTI 5 GHz	AT/VLA 5 GHz	Total 5 GHz	LLS (kpc)	α PTI	P_{core}/P_{tot}	P_{core}/P_{lobe}
(1)	(2)	(3)	(4)	(5)	(6)	(7)	(8)	(9)	(10)
149–G19	E/S0	−21.6	<21.97		23.56			<0.025	<0.026
013–G12	S0	−21.3	<21.40		22.64			<0.058	<0.062
NGC 547	E	−21.4	22.79		24.15		+0.46	0.043	0.045
NGC 612*	S0	−21.7	22.66	22.67	24.57	450	+0.26	0.012	0.012
NGC 636	E	−19.8	<20.57		20.65			<0.833	<5.0
NGC 641	E	−21.5	22.00	21.91	22.91	50	+0.58	0.124	0.142
NGC 741	E	−22.2	21.86		23.18	44	−0.28	0.047	0.050
NGC 1052	E/S0	−20.3	22.92		22.80	3	+1.09	1.35	
NGC 1209	E	−20.4	21.42	21.12	21.25		+0.22	1.48	
NGC 1316*	S0	−22.4	<20.38	21.16	24.57	367		<0.0001	<0.0001
NGC 1399*	E	−21.0	20.81	20.56	22.09	22	+0.22	0.053	0.056
NGC 1407	E	−21.3	<20.50		21.44			<0.114	<0.128
NGC 1453	E	−21.4	21.78		21.75		−0.12	1.06	
NGC 1587	E	−20.9	21.43		22.40		+0.27	0.108	0.121
NGC 1600	E	−22.1	<21.38		22.02	7		<0.227	<0.294
NGC 1947	S0	−19.1	<20.00		20.56			<0.278	<0.385
NGC 2110	E	−19.1	21.66	22.07	22.29	0.6	+0.33	0.236	0.309
NGC 2640	S0	−19.4	20.59	20.70	20.54		+0.46	1.14	
NGC 2663	E	−21.7	22.02	22.06	22.87		+0.29	0.139	0.161
NGC 2911	S0	−20.3	21.91	22.49	22.45	<0.4	−0.21	0.283	0.395
NGC 2986	E	−20.8	<20.68		21.50			<0.152	<0.179
NGC 3078	E	−20.5	22.15	22.08	22.14		+0.26	1.04	
NGC 3100*	E	−21.0	22.24	22.86	22.79	0.3	−0.25	0.280	0.388
NGC 3250	E	−21.1	<20.84	<20.13	21.46			<0.238	<0.312
NGC 3258	E	−20.5	<20.83	20.73	21.85	7		0.096	0.106
NGC 3268	E	−20.5	21.41	21.49	21.57	<0.8	−0.45	0.679	2.11
263–G48	S0	−21.0	<20.86	20.46	21.46	3		0.250	0.338
NGC 3309	E	−21.4	<21.18	<20.96	21.63	4		<0.357	<0.556
NGC 3557*	E	−22.0	21.48	21.18	22.66	24	+0.56	0.067	0.072
NGC 3706	S0	−21.1	<20.99	21.19	21.57	12		<0.263	<0.357
NGC 4373	E	−21.8	21.02	21.44	21.40	<0.3		0.417	0.714
NGC 4550	E/S0	−18.3	<20.13	19.35	20.94			<0.153	<0.181
NGC 4636	E/S0	−19.8	<19.86		20.81	2		<0.111	<0.125
NGC 4696	S0	−21.9	21.41	21.90	23.30	8	−0.45	0.013	0.013
NGC 4756	E	−20.4	<21.26		22.56			<0.051	<0.054
NGC 4760	E	−21.7	22.22		23.25		−0.24	0.093	0.103
NGC 4936	E	−21.6	21.90		22.24		−0.34	0.452	0.825
323–G93	S0	−20.4	21.58	21.66	21.86	<0.2	+0.27	0.525	1.11
NGC 5044	E	−21.3	21.52		21.59		+0.38	0.849	5.60
NGC 5077	E	−20.6	22.62		22.40	<0.5	+0.40	1.64	

Table 7 – *continued*

Name		Abs. mag	Log P (W/Hz) PTI 5 GHz	AT/VLA 5 GHz	Total 5 GHz	LLS (kpc)	α PTI	P_{core}/P_{tot}	P_{core}/P_{lobe}
(1)	(2)	(3)	(4)	(5)	(6)	(7)	(8)	(9)	(10)
NGC 5090	E	−21.1	23.11	22.76	23.55	211	+0.49	0.366	0.577
NGC 5128	E	−21.0	22.15	22.19	23.44	125		0.051	0.054
NGC 5140	S0	−21.0	21.86	21.92	22.09		+0.12	0.589	1.43
IC 4296*	E	−21.9	22.88	22.73	23.60	514	+0.65	0.187	0.230
NGC 5419*	E	−22.3	21.45	21.73	23.14	234	<−0.05	0.021	0.021
NGC 5846	S0	−20.8	20.68	20.47	20.68			1.00	
137–G45	E	−21.1	21.48	21.19	21.85			0.424	0.737
NGC 6730	E	−20.8	22.21	22.11	22.39			0.657	1.91
NGC 6758	E	−20.9	<21.04		21.79			<0.179	<0.217
232–G21	S0	−19.1	<21.21		22.03			<0.152	<0.179
NGC 6861	E	−20.9	21.00	20.91	21.51			0.300	0.429
NGC 6868	E	−21.4	22.08	22.01	22.29		+0.07	0.614	1.59
IC 4991	S0	−22.3	<21.53	20.83	22.13	22		<0.250	<0.338
NGC 6958	E	−20.6	21.36	21.45	21.62	<0.2	+0.16	0.545	1.20
IC 5063	S0/a	−20.6	21.82		23.07		−2.03	0.056	0.059
NGC 6987	E/S0	−20.9	22.16	22.23	22.53		+0.06	0.424	0.736
NGC 7002	E	−21.7	22.47	22.45	22.75		+0.49	0.516	1.07
NGC 7049	S0	−20.9	21.15	21.25	21.52		−0.10	0.422	0.730
NGC 7097	E	−19.9	21.61	21.33	21.33	<0.2		1.89	
NGC 7213	S0	−20.8	22.22	22.17	22.16		+0.49	1.13	
NGC 7216	E	−19.8	21.89	21.95	22.03		+0.14	0.727	2.67
IC 1459 *	E	−21.0	22.54	22.79	22.81	<0.1	−0.48	0.535	1.15

Columns.
(1) Object name.
(2) Galaxy type.
(3) Absolute magnitude M_B, corrected for Galactic extinction.
(4), (5), (6) Radio power at 5 GHz: PTI core, VLA core and total power respectively.
(7) Largest linear size (LLS) of extended radio emission (omitted for galaxies without extended structure).
(8) Spectral index of PTI core, calculated as described in the text.
(9) Ratio of PTI core flux to total 5-GHz flux.
(10) Core-to-lobe ratio at 5 GHz (where lobe flux is defined as total flux minus core flux).

Table 8. Radio power and other derived quantities for sample B.

Name		Abs. mag	Log P (W/Hz) PTI 5 GHz	VLA 5 GHz	Total 5 GHz	LLS (kpc)	α PTI	P_{core} /P_{tot}	P_{core} /P_{lobe}
(1)	(2)	(3)	(4)	(5)	(6)	(7)	(8)	(9)	(10)
0005–199	E	–22.1	23.50	23.57	24.82	484	+0.53	0.048	0.051
0007–325	E	–20.9	23.40	23.45	23.63	3	+0.59	0.593	1.46
0013–240	S	–20.4	23.81	24.18	24.26	<1.3	–0.57	0.351	0.544
0013–316	E	–21.8	<23.01	23.01	24.42	100		<0.039	<0.041
0023–333	E	–22.2	22.81	22.70	24.32	140	+0.62	0.032	0.033
0038–210	E	–20.6	<22.89	24.40	24.71	18		<0.015	<0.015
0048–233	E	–20.9	<23.11	<23.40	24.70	181		<0.026	<0.026
0131–367*	S0	–21.7	22.66	22.67	24.57	450	+0.26	0.012	0.012
0155–212	E	–21.5	24.21	24.24	25.04	315	–0.07	0.146	0.171
0229–208	E	–22.0	24.11	24.16	24.86	339	+0.53	0.179	0.218
0247–207	E	–22.5	23.50	23.52	24.64	411	+0.56	0.072	0.078
0257–398	E	–22.1	<22.54	<22.54	24.57	39		<0.009	<0.009
0307–305	E	–21.4	<22.65	22.42	24.53	178		<0.010	<0.010
0312–343	E	–21.7	23.33	23.33	24.27	195	<–1.02	0.114	0.128
0320–374*	S0	–22.4	<20.38	21.16	24.57	367		<0.0001	<0.0001
0332–391	E	–21.9	23.03	22.99	24.50	365	+0.22	0.034	0.035
0336–355*	E	–21.0	20.81	20.56	22.09	22	+0.22	0.053	0.056
0344–345	E	–20.9	23.56	23.34	24.71	397	+0.40	0.071	0.076
0344–291	DB	–21.4	23.77	24.04	24.92	77	+0.04	0.070	0.076
0349–278	E	–21.2	23.13	23.11	25.25	475	+0.79	0.007	0.008
0434–225	E	–22.9	<22.73	22.90	24.54	172		<0.015	<0.016
0446–206	E	–21.2	<22.71	22.95	24.34	127		<0.023	<0.024
0449–175	E	–21.4	22.22	22.28	23.77	154	+0.74	0.029	0.030
0452–190	E	–21.7	22.81	22.82	23.70	40	+0.13	0.128	0.147
0453–206	E	–21.6	22.79	22.95	24.60	28	+0.08	0.016	0.016
0511–305	E	–20.8	22.84	22.81	24.69	849	+0.76	0.014	0.015
0521–365	N	–21.0	25.10	24.92	25.73	35	+0.65	0.232	0.303
0523–327	D	–22.3	23.21	23.22	24.61	353	+0.38	0.040	0.042
0533–377	E	–21.5	23.41	23.36	24.45	206	+0.38	0.092	0.102
0546–315	E	–21.5	<23.32	23.32	24.77	159		<0.036	<0.037
0546–329	E	–21.7	22.89	22.92	23.76	452	+0.34	0.137	0.158
0548–322	BL	–22.0	23.53	23.80	24.32	40	+0.24	0.162	0.193
0548–317	E	–21.4	<22.08	<22.08	23.94	18		<0.014	<0.014
0618–371	DB	–20.7	22.60	22.48	24.41	81	+0.20	0.015	0.016
0625–354	E	–21.1	24.46	24.54	25.09	156	+0.24	0.236	0.309
0634–205	E	–20.9	22.86	22.86	25.33	963	+0.26	0.003	0.003
0712–349	E	–21.1	23.07	22.96	23.79	36	+0.29	0.192	0.237
0718–340	E	–20.8	22.69	22.67	24.17	54	+0.30	0.033	0.034
0940–304	E	–21.9	22.95	23.10	23.71	64	+0.46	0.173	0.210
0958–314*	E	–21.0	22.24	22.86	22.79	0.3	–0.25	0.279	0.388
1002–320	E	–20.8	<22.87	<22.87	24.53	187		<0.022	<0.022
1043–290	E	–21.8	23.48	23.54	24.25	323	+0.27	0.171	0.207
1053–282	E	–21.7	23.98	23.89	24.78	58	+0.48	0.161	0.191
1056–360	E	–21.7	23.75	23.67	24.68	503	+0.29	0.118	0.133
1107–372*	E	–22.0	21.48	21.18	22.66	24	+0.56	0.067	0.072
1123–351	E	–21.4	23.00	23.14	24.19	93	+0.20	0.065	0.070
1142–341	D	–22.0	<22.65	23.12	23.99	49		<0.045	<0.048
1144–327	D	–22.0	<22.54	22.84	24.12	182		<0.026	<0.027
1228–335	D	–21.7	23.05	22.88	24.09	119	+0.29	0.090	0.099
1251–289	E	–22.7	22.90	<22.80	24.18	23	+0.06	0.052	0.055
1254–300	D	–21.8	<22.44	<22.44	24.31	73		<0.014	<0.014
1257–253	E	–21.3	23.18	23.10	24.33	125	+0.38	0.070	0.075
1258–321	E	–21.4	22.71	22.63	23.53	32	+0.38	0.155	0.183
1306–241	S	–18.4	22.39	22.86	22.88	<0.3	–0.93	0.326	0.483
1323–271	E	–21.0	22.93	22.73	24.25	151	+0.51	0.048	0.050
1329–328	D	–21.2	<22.52	<22.43	24.25	82		<0.018	<0.019
1333–336*	E	–21.9	22.88	22.73	23.60	514	+0.65	0.187	0.230
1344–241	S0	–20.3	<21.67	<21.44	23.14	148		<0.034	<0.035
1354–251	E	–20.8	22.27	22.13	23.91	66	<–0.03	0.023	0.024
1400–337*	E	–22.3	21.45	21.73	23.14	234	<–0.05	0.021	0.021

Table 8 – *continued*

Name		Abs. mag	Log P (W/Hz) PTI 5 GHz	VLA 5 GHz	Total 5 GHz	LLS (kpc)	α PTI	P_{core}/P_{tot}	P_{core}/P_{lobe}
(1)	(2)	(3)	(4)	(5)	(6)	(7)	(8)	(9)	(10)
1404–267	E	−20.5	23.48	23.36	23.51	4	−0.09	0.927	12.7
1413–364	E	−20.4	<22.73	<22.73	24.92	366		<0.006	<0.007
1514–241	BL	−21.2	24.84	25.21	25.05	<1.1	−0.13	0.629	1.70
1521–300	E	−19.8	23.25	23.10	23.50	2	+0.47	0.570	1.33
1928–340	E	−21.2	<22.95	23.57	24.53	141		<0.026	<0.027
1929–397	E	−22.7	<22.73	23.16	25.01	229		<0.005	<0.005
2013–308	E	−22.9	23.11	23.18	24.62	431	+0.47	0.031	0.032
2031–359	E	−22.7	23.62	23.24	24.94	55	−0.05	0.049	0.051
2040–267	E	−21.8	22.72	22.95	24.40	303	+0.60	0.021	0.021
2058–282	E	−21.0	23.26	23.32	24.74	494	+0.22	0.033	0.034
2059–311	E	−21.8	22.68	22.70	23.75	149	<−0.71	0.090	0.093
2104–256	E	−21.2	23.20	23.27	25.06	378	+0.47	0.014	0.014
2128–388	E	−20.3	22.16	22.12	23.42	43	+0.11	0.054	0.057
2158–380	E	−21.3	<22.02	<22.02	24.10	87		<0.009	<0.009
2206–237	E	−20.4	23.98	25.20	25.15	<1.7	−1.43	0.069	0.074
2209–255	E	−21.4	23.59	23.58	24.30	37	+0.01	0.198	0.248
2225–308	E	−21.2	23.16	23.24	24.29	80	+0.75	0.074	0.079
2236–176	E	−22.3	<22.80	23.02	24.75	201		<0.011	<0.011
2236–364	D	−21.9	23.37	22.69	24.28	31	+0.34	0.122	0.138
2254–367*	S0	−21.0	22.54	22.79	22.81	<0.1	−0.48	0.535	1.15
2331–240	E	−20.7	24.46	24.67	24.65	<0.9	+0.28	0.650	1.86
2333–327	E	−22.2	<22.42	22.79	23.83	171		<0.039	<0.041
2350–374	E	−22.5	<23.11	<23.00	24.72	279		<0.024	<0.025
2353–184	E	−21.5	<22.70	<23.00	24.49	63		<0.017	<0.017
2354–350	D	−22.1	<22.42	22.49	23.68	33		<0.054	<0.058

Columns.
(1) Object name. Galaxies marked * also belong to the low-power sample. (2) Galaxy type. (3) Absolute magnitude M_B, corrected for Galactic extinction. (4), (5), (6) Radio power at 5 GHz: PTI core, AT/VLA core and total power respectively. (7) Largest linear size (LLS) of extended radio emission, based on private communication by R. D. Ekers et al. (8) Spectral index of PTI core. (9) Ratio of PTI core flux to total 5-GHz flux. (10) Core-to-lobe ratio at 5 GHz (where lobe flux is defined as total flux minus core flux).

3.4 Core luminosity function

Tables 7 and 8 list various absolute quantities calculated for our two samples on the basis of the distance adopted for each galaxy. We can now derive the PTI core luminosity function and investigate the relationship between core and total power for these galaxies.

Since we have both detections and upper limits in our sample, we have used survival analysis methods (Feigelson & Nelson 1985; Schmitt 1985) to calculate the fractional luminosity function $F(P_{\rm PTI})$ of the cores at 5 GHz. For this and subsequent calculations we used the ASURV statistical package (LaValley, Isobe & Feigelson 1992), which implements the methods presented by Feigelson & Nelson (1985) and Isobe, Feigelson & Nelson (1986). $F(P_{\rm PTI})$, plotted in Fig. 7, represents the fraction of galaxies with PTI core powers in the range $P \pm \Delta P$ in a given sample. The low- and medium-power samples show well-defined peaks near 10^{21} and 10^{23} W Hz^{-1} respectively, suggesting that the cores are typically 100 times more powerful in the medium-power than in the low-power galaxies. This is confirmed by Fig. 8, in which we plot the core and total 5-GHz luminosities for individual sources.

The core radio power P_c and total power P_t are already known to be related for high-power radio galaxies. Fabbiano et al. (1984) found $P_c \propto P_t^{0.75\pm0.05}$ for a complete sample of 43 3CR radio galaxies, while Giovannini (1985) derived $P_c \propto P_t^{0.57\pm0.06}$ for a sample of 138 radio galaxies taken from the 3CR and Bologna catalogues. Both these studies covered galaxies with high radio luminosity, and the reason for the discrepancy in the power-law index is not clear.

For the 140 galaxies in our combined sample, we did a regression analysis, taking into account the upper limits to the core flux, and found $P_c \propto P_t^{0.73\pm0.05}$. Thus the correlation between core and total power found by other authors for 3CR galaxies extends to radio luminosities as low as 10^{21} W Hz^{-1}.

3.5 Variability

We noted in Section 2.2.3 that the calibrators used in this experiment varied in flux by up to 10 per cent over a 3-yr interval. We now test whether the cores of our target galaxies are also variable.

To examine this, we used our own PTI and AT measurements, plus the VLA core fluxes measured by Sadler

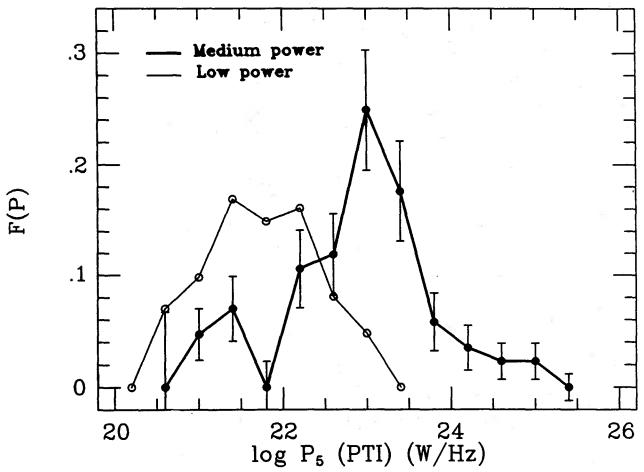

Figure 7. Fractional radio luminosity function $F(P)$ for PTI core sources at 5 GHz. The two samples are shown separately.

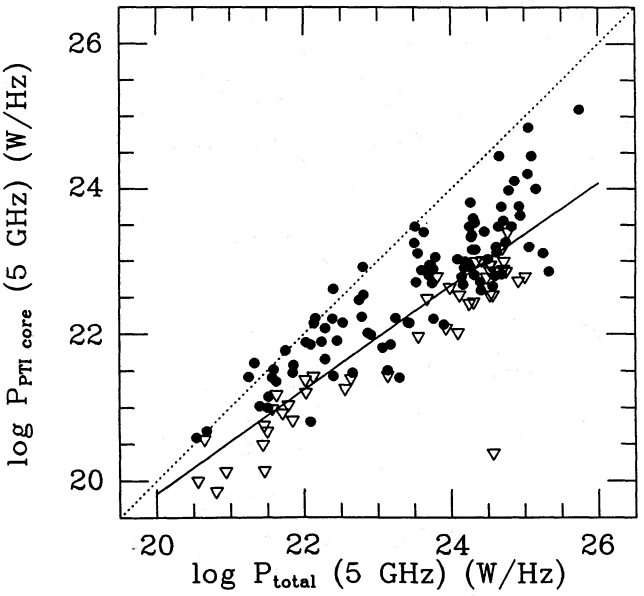

Figure 8. Relation between PTI and total radio power at 5 GHz for the combined sample. Again, triangles show PTI upper limits. Note the very low upper limit for the core emission from Fornax A. The solid line is the linear regression $\log P_c \propto 0.71 \log P_t$ discussed in the text, while the dotted line shows the relation $P_c = P_t$.

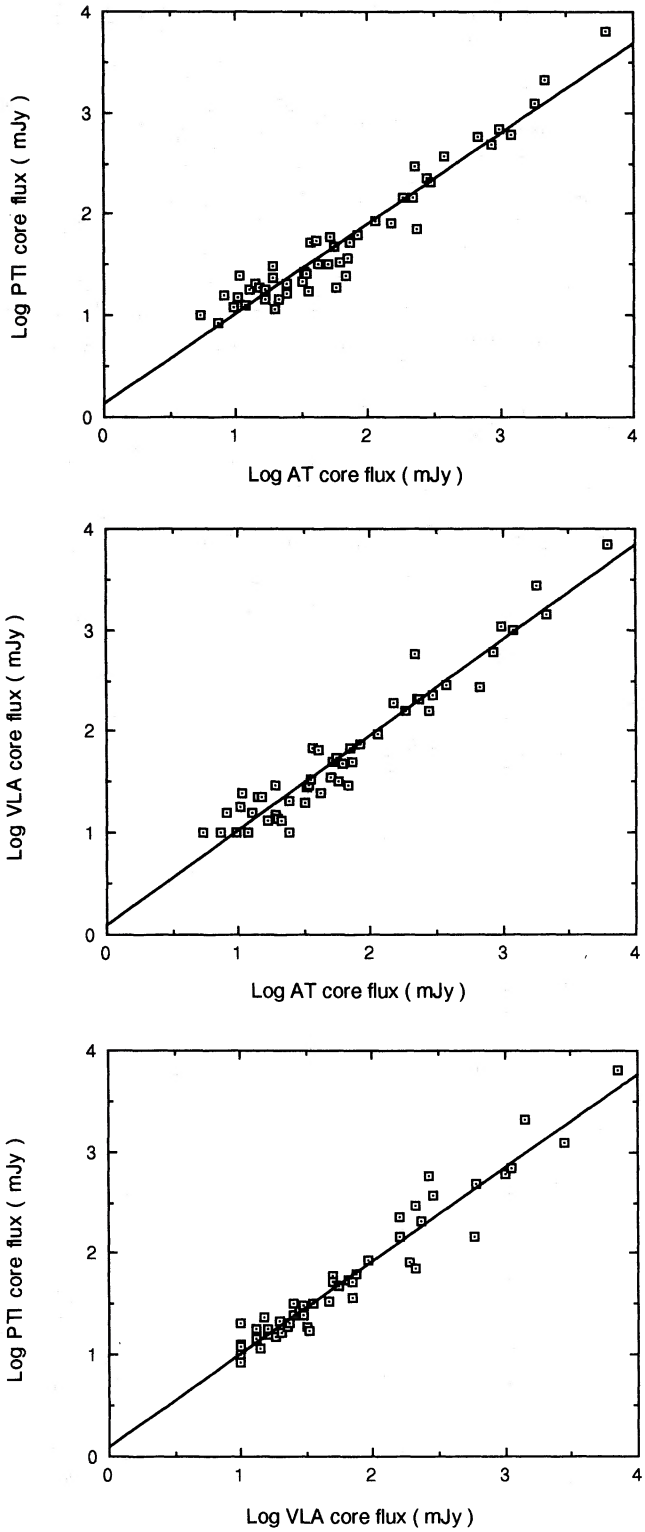

Figure 9. Regression relations between PTI, VLA and AT core fluxes for galaxies with detected cores.

et al. (1989) and Ekers et al. (1989) during 1979–84. We constructed scatter diagrams for the core fluxes of 50 sources which were measured at epochs typically 6–7 yr apart, and compared them with similar scatter diagrams obtained from PTI and AT measurements separated by only one or two years. Comparison of the arcsec-scale VLA/AT flux with the smaller scale PTI flux is valid because we have already shown in Section 3.3 that most core sources in our sample are unresolved.

Fig. 9 shows the resulting correlation diagrams for the three possible combinations PTI–VLA, PTI–AT and VLA–AT. From the slopes of the least-squares regression line, the PTI fluxes are consistently lower by 8 and 11 per cent than the corresponding VLA and AT fluxes respectively. The correlation coefficients are high (0.96) in all three plots.

As discussed in Section 3.3, a likely explanation for the higher fluxes measured at the AT and the VLA is that the

synthesis instruments, with their lower angular resolution, include some of the larger-scale structure in their 'core' measurements. This is supported by the fact that the VLA core fluxes in Fig. 9 tend to be about 6 per cent lower than the corresponding AT fluxes, consistent with the somewhat lower resolution of the AT in these observations.

The standard deviation of regression averages 0.180 in the log, equivalent to a linear dispersion of ~40 per cent about the regression line. Thus we find that the core variability is <40 per cent over 2.5 decades of core flux on both short (1–2 yr) and medium (6–10 yr) time-scales. This is consistent with the maximum variability of ~10 per cent found for our calibrators – much of the variance in our correlation diagrams is due to measurement error, which will obscure smaller intrinsic flux changes.

In galaxies where the radio emission is dominated by a compact core ($P_c \gg 0.5P_t$), the measured flux does not depend on the resolution, and we can supplement our own observations with lower-resolution archival data from other observers to extend the time coverage.

Fig. 10 shows data for three galaxies that have been observed for at least 20 yr. Data points at 5 GHz are from Heeschen (1970), Whiteoak (1970), Shimmins & Bolton (1972), Ekers & Ekers (1973), Disney & Wall (1977), van Breugel et al. (1981), Ekers, Fanti & Miley (1983), Sadler (1984c) and Wrobel & Heeschen (1984). The results suggest that these sources vary monotonically on time-scales of decades, though outbursts like that in NGC 1052 in 1975–76 clearly occur on much shorter time-scales.

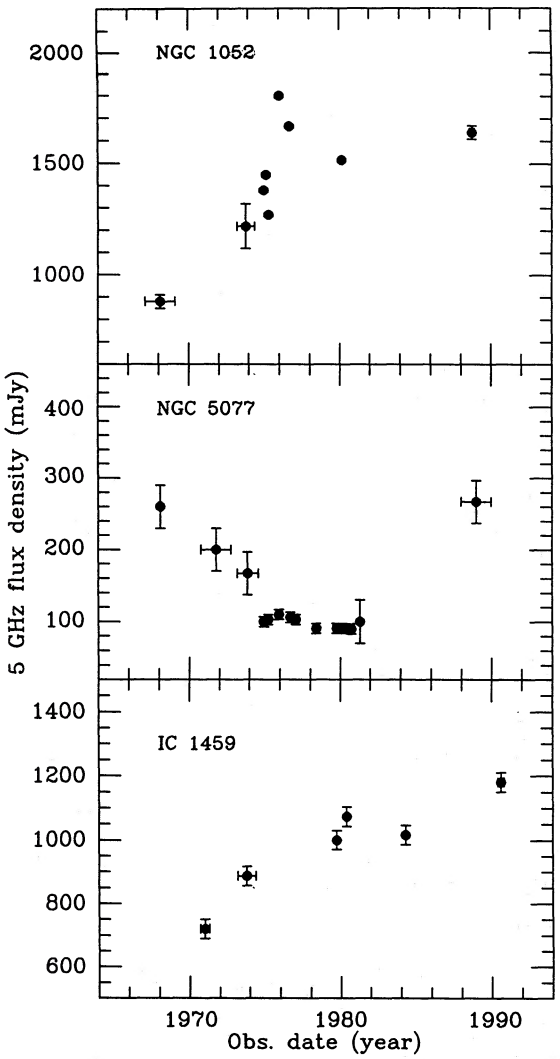

Figure 10. 5-GHz flux densities measured during 1968–91 for (a) NGC 1052, (b) NGC 5077, (c) IC 1459.

If the core flux is time-varying and the fluxes at different frequencies are not measured simultaneously, this may affect the measured spectral index. In our sample, however, the results from multiple observations of programme objects and calibrators suggest that the typical intrinsic variability is no more than 10 per cent over 2–3 yr, and this is unlikely to have a serious effect on the measured spectral index.

4 DISCUSSION

4.1 Mechanisms for the observed core spectra

We need to explain the predominance of positive spectral indices in the core spectra (as shown in Section 3.3), and to account for the remarkably similar distributions of spectral index in two samples of very different luminosity. A review of the basic theoretical framework used to interpret these sources is given by Kellermann & Pauliny-Toth (1981). Some relevant mechanisms are discussed below:

(i) *The intrinsic radiation spectrum.* It seems unlikely that any realistic distribution of relativistic electron energies in a uniform source could produce the observed spectral distribution. A flat electron-energy spectrum with continuous injection and/or re-acceleration could produce a flat radio spectrum, but there are formidable difficulties in maintaining such a spectrum against synchrotron radiation losses which, over time, make the spectrum increasingly negative at higher frequencies.

Thermal emission from H II regions can be ruled out, since the brightness sensitivity of the PTI is 10^5 K, whereas the electron temperature of H II regions does not usually exceed 10^4 K.

(ii) *Scattering on electron density irregularities.* This mechanism increases the apparent angular size of a compact source in proportion to the square of the wavelength. Since the angular resolution of the PTI decreases linearly with wavelength, the observed ratio of source diameter to fringe spacing should increase linearly with wavelength, i.e. by a factor of 3.65 between 8.4 and 2.4 GHz. Thus, if the effect is large, a source that is unresolved at the higher frequency might be partly resolved at the lower frequency, with a consequent decrease in apparent flux density. It is hard to quantify the effect on the observed spectral index without knowing the intrinsic spectrum and source diameter, though the good agreement between our interpolated 5-GHz fluxes and the arcsec-scale VLA/AT core fluxes suggests that any effect must be small.

(iii) *Synchrotron self-absorption.* Synchrotron self-absorption in extragalactic radio sources was first considered in detail by Kellermann & Pauliny-Toth (1969), who pointed out that positive spectral indices are quite common amongst the most luminous radio sources at centimetre wavelengths. For a sample of (mainly) luminous quasi-stellar objects (QSOs), they inferred magnetic fields in the range

10^{-5}–10^{-3} G and brightness temperatures in the range 10^{11}–10^{12} K.

Since we find that many lower-luminosity radio galaxies also have cores with positive spectral indices, it seems likely that the same mechanism is responsible, but, although self-absorption can account for the spectral turnover in the most compact sources with brightness temperatures close to the 10^{12} K Compton limit, there is evidence that significantly different physical conditions exist in the lower-luminosity sources.

Most of our sources are unresolved with the PTI, and so we lack the angular size measurements needed to estimate brightness temperature and sufficient multifrequency observations to define the spectral peak. Thus we cannot estimate directly the magnetic field needed to produce synchrotron self-absorption in our sources. If we assume approximate equipartition of energy between the magnetic field and relativistic particles, we can use the standard synchrotron formulae to show that a typical source in the low-power sample A (with a core flux density of ~ 20 mJy, a distance of ~ 30 Mpc and a self-absorption turnover frequency above 5 GHz) must have a magnetic field of at least 0.1 G, an angular size $< \sim 0.2$ mas and a brightness temperature of order 3×10^{10} K. In particular, magnetic fields of order 10^{-3} G, the highest found in the Kellermann & Pauliny-Toth analysis, are possible only if the energy in relativistic particles exceeds that in the magnetic field by many orders of magnitude, with still smaller angular sizes resulting (< 0.1 mas).

For two members of our low-power sample, angular sizes are known from VLBI. The VLBI image of NGC 1052 published by Jones, Wrobel & Shaffer (1984) shows that most of the emission at 5 GHz comes from an inner jet ~ 5 mas long. Since the jet is unresolved in the narrow dimension, it is not possible to compute a brightness temperature. The adoption of a turnover frequency of 5 GHz (their fig. 6), and the assumption of equipartition of magnetic and particle energies, gives a magnetic field of ~ 0.1 G and an angular width for the jet of ~ 0.2 mas (0.02 pc).

Similar conclusions follow from a VLBI image of NGC 5128 (Meier et al. 1993), which has a bright ~ 30-mas jet (again unresolved in the perpendicular direction). Equipartition arguments again yield a magnetic field of ~ 0.1 G and a transverse jet width of ~ 0.2 mas (0.01 pc). The synchrotron lifetime of electrons radiating at 5 GHz in a 0.1-G field is ~ 10 yr.

Even with the likelihood of additional complicating factors (such as multiple components within each source, with different turnover frequencies and angular sizes), the simple considerations outlined here imply that, in the synchrotron self-absorption picture, either the magnetic fields in low-luminosity radio galaxy cores are substantially stronger than previously thought, or they are well below equipartition values, with the energy in relativistic particles exceeding magnetic energy by several orders of magnitude. In either case, the angular size of the cores or core components is required to be less than 1 mas. Additional high-resolution measurements spanning a wider range of frequencies are needed to consolidate these preliminary conclusions.

(iv) *Free–free absorption in a plasma.* Phillips et al. (1986) have shown from optical emission-line measurements that most E/S0 galaxies contain at least 10^3–10^4 $M_\odot$ of low-temperature (10^4 K) ionized gas, most of it within a few hundred parsecs of the centres of the galaxies. It is therefore possible that the positive spectral index seen in the cores is caused by the onset of free–free absorption in this gas. We can use our observed median spectral index of 0.3 between 2.3 and 8.4 GHz to derive an optical depth to free–free absorption, assuming that the spectrum peaks near 8.4 GHz and that the radiated spectrum has a spectral index of -0.50.

We derive an optical depth of 1 at 2.3 GHz, and an emission measure of 1.6×10^7 cm^{-6} pc. A uniformly filled sphere of 10^4 $M_\odot$ of ionized hydrogen would need to be confined to ~ 4 pc in radius with an electron density of $\sim 2 \times 10^3$ cm^{-3} to achieve this emission measure. This does not seem unreasonable in the light of the Phillips et al. result, bearing in mind the possibility of substantially non-uniform distributions. Filling factors considerably less than unity would not only reduce the amount of ionized gas needed, but allow the occupied volume to increase. We clearly need core spectra over a wide range of frequencies (say 1.5–20 GHz), taken within a short time interval, to define the optically thick and thin regions of the spectrum unambiguously. This would allow us to determine both the radiated spectrum and the optical depth at frequencies in the optically thick regime.

It is worth noting that the free–free absorption observed in the nuclear radio components of the starburst galaxies NGC 253 (Reynolds & Harnett 1983) and M82 (Hargrave 1974) may be related to the detection of hydrogen recombination lines in both these galaxies (Shaver, Churchwell & Rots 1977; Seaquist & Bell 1977). Shaver et al. (1977) suggest that these lines arise from amplification of the nuclear component by stimulated emission within the intervening ionzied gas.

For NGC 253, Seaquist & Bell compute an optical depth (negative) for the 6.1-GHz H102α line of $(-)0.014$ if it is due to amplified emission from the nucleus. This is comparable to the optical depth at the same frequency due to free–free absorption of the nuclear source (which shows a turnover near 1 GHz), suggesting that substantial free–free absorption should produce detectable recombination lines in the galaxy samples considered here, at frequencies near or just above the turnover in the spectrum.

To sum up, both synchrotron self-absorption and free–free absorption might, plausibly, produce the observed core spectrum, though synchrotron self-absorption would be ruled out if the sources were shown to be larger than ~ 1 mas. Further measurements are therefore needed for a definitive answer.

4.2 Orientation effects and beaming

Relativistic beaming models are an important part of unified schemes for radio galaxies, BL Lac objects and quasars. The basic idea (e.g. Scheuer & Readhead 1979; Blandford & Königl 1979) is that the brightest extended double sources (like Cygnus A) are intrinsically powerful, while the brightest core-dominated compact sources arise in a small fraction of intrinsically fainter objects which are brightened by Doppler boosting because material moving at relativistic velocities happens to be viewed almost head-on. Readhead, Pearson & Barthel (1988) discuss some of the main assumptions and predictions of beaming theory.

The application of relativistic beaming to low-luminosity radio galaxies (as opposed to quasars and FR II radio

galaxies) has been largely neglected (due, we suspect, to a lack of complete samples of core measurements for FR I galaxies). Ulrich & Meier (1984) used the VLA to search for radio cores in 18 medium-power radio galaxies and found a shortage of weak sources with strong cores, which became even more pronounced if relativistic beaming was assumed to operate. They point out, however, that this may be a selection effect because quasars (many of which have strong cores) were excluded from their sample.

The two samples that form the basis of this paper are flux limited in both their total and core fluxes. A commonly quoted treatment of the effects of relativistic beaming on the radio source statistics is that of Orr & Browne (1982), who postulate an intrinsic core-to-lobe ratio R_t, a Lorentz factor γ and a random orientation on the sky of the inner (assumed highly relativistic) jets. We can use their equations 2 and 3 to derive the probability of R lying between R and $R+\mathrm{d}R$, and hence the expected distribution of R in a sample of sources. The effect of increasing γ is to increase the probability of higher R, but its effect on the overall distribution is hardly noticeable for $\gamma > 2$.

In our sample, we calculate the core-to-lobe ratio R by assuming that the lobe flux is equal to the total flux minus the core flux. Figs 11 and 12 show the distribution of R for the low-power (median $R=0.204$) and medium-power (median $R=0.051$) samples respectively. It is clear that the distributions are different for the two samples, and this is confirmed by ranking tests which show that the two distributions have a probability of only 0.0001 of being drawn from the same population.

We have evaluated the probability distributions for a range of R_t and R, and compared them with the observed distributions. Fig. 13 shows the results for the medium-power sample with the computed distribution (horizontal hatching) evaluated for $R_t=0.056$. Selecting different values for R_t merely moves the whole distribution along the x axis. It is clear that a unique R_t which applies to all radio galaxies cannot reproduce the observed distribution. If we allow R_t to have a range of values with a quasi-Gaussian distribution of five steps of 0.5 dex with $0.003\,16 < R_t < 0.316$, then we have the predicted distribution of R shown in Fig. 14. Such a distribution (which again can be shifted along the x axis according to the central value of R_t) reproduces the observed distribution reasonably well. In this case, shifting the central value of R_t to the right by dex 0.5 would fit the measured R better, but the upper limits also need to be taken into account. Once we relax the assumption of a single fixed R_t and allow it to have a range of values, however, it is equally valid to assume that there is an even wider intrinsic range in R_t and no relativistic beaming.

In summary, we find that relativistic beaming models with a fixed intrinsic core-to-lobe ratio R_t cannot reproduce the observed distribution of core-to-lobe ratios in our sample. Such models can give distributions consistent with observations if we allow R_t to take a range of values, but a picture in

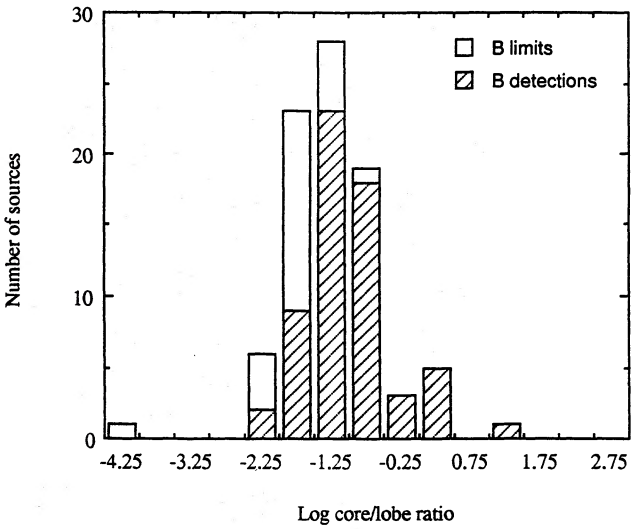

Figure 12. Histogram of core-to-lobe ratio for the medium-power sample.

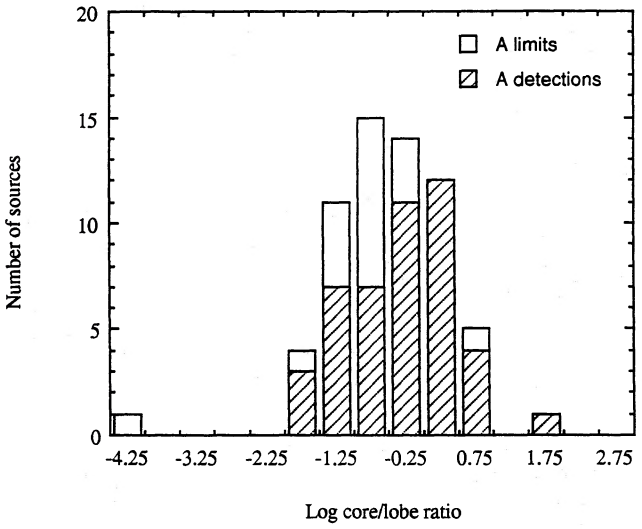

Figure 11. Histogram of core-to-lobe ratio for the low-power sample.

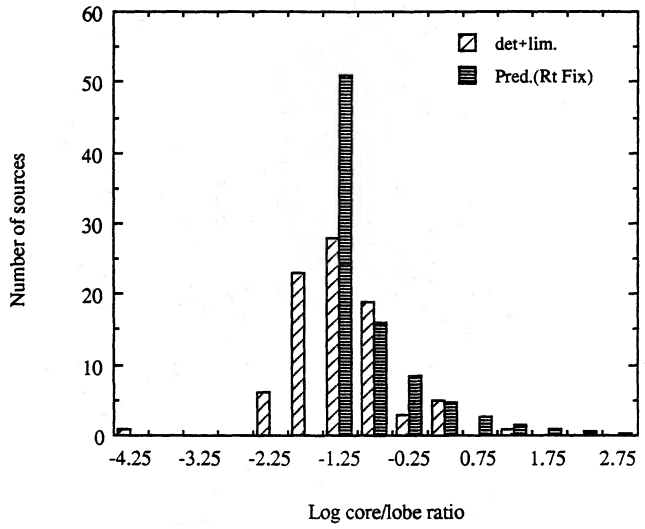

Figure 13. Histogram of observed core-to-lobe ratios at 5 GHz, and ratio predicted by a beaming model with fixed $R_t=0.056$.

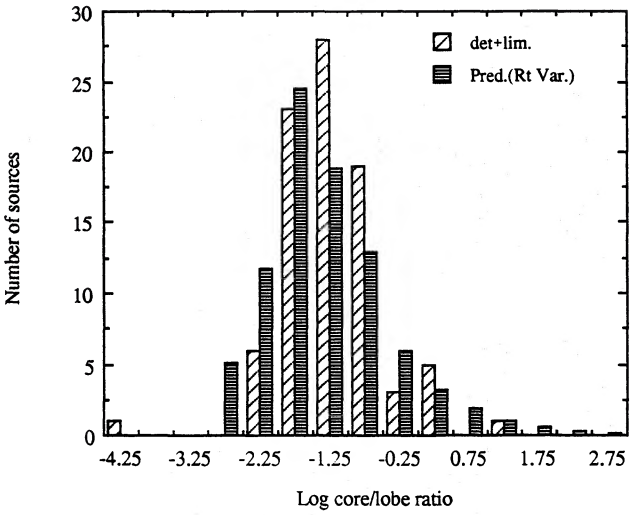

Figure 14. As Fig. 13, but with R_t allowed to take a range of values with a maximum at 0.032.

which the sources are not relativistically beamed but simply have a large intrinsic range in core-to-lobe ratio appears equally valid.

4.3 Do all radio galaxies have cores?

Since most of the galaxies we have observed show parsec-scale cores, our failure to detect the nearby radio galaxy NGC 1316 (Fornax A) with the PTI is puzzling. It suggests that there may be a subset (up to 20–30 per cent) of radio galaxies in which the core has either switched off or is very highly self-absorbed. Alternatively, Fornax A may be related to the compact steep-spectrum radio sources.

5 CONCLUSIONS

Many nearby elliptical and S0 galaxies contain parsec-scale radio cores that appear qualitatively similar (in both size and spectral index) to the active nuclei of radio galaxies and quasars. At least 70 per cent of early-type galaxies with radio powers above 10^{21} W Hz^{-1} appear to have such a core.

In general, we find that radio galaxies become increasingly core dominated at lower luminosities ($P_{\rm core} \propto P_{\rm total}^{0.7}$). This is the opposite of what would be expected if core-dominated objects represented the beamed subset of a population with constant core-to-lobe ratio, so it appears that most low-power cores do not produce an extended radio source. In the weakest radio sources we have studied, almost all the radio emission comes from the central few parsecs.

There are, however, some stronger core-dominated sources (e.g. IC 1459) which show far less extended emission than expected for their core power. It is not yet clear whether these are beamed objects, or represent a genuine class of higher-power 'naked cores'. VLBI imaging would be valuable to measure v/c and test for superluminal motion.

Most of the cores we have observed have a flat or rising spectrum between 2.3 and 8.4 GHz, with a median spectral index of $+0.3$. Synchrotron self-absorption is not ruled out as a means of producing such a spectrum, but would require that the cores are very small (<1 mas) and that the magnetic fields in the nuclei of low-luminosity radio galaxies are much stronger than previously thought (unless equipartition does not apply). Free–free absorption is perhaps a more likely mechanism, especially since the inner regions of most early-type galaxies are known to contain modest amounts of ionized gas. Measurements of the core spectra over a wider range of frequencies are needed for further progress, and a search for recombination lines in some of these galaxies might provide a decisive test.

ACKNOWLEDGMENTS

We thank Alan Roy for assisting with several observing runs, and R. T. Schilizzi for carrying out the 12.2-GHz observations.

REFERENCES

Baars J. W. M., Genzel R., Pauliny-Toth I. I. K., Witzel A., 1977, A&A, 61, 99
Birkinshaw M., Davies R. L., 1985, ApJ, 291, 32
Blandford R. D., Königl A., 1979, ApJ, 232, 34
Cordey R. A., 1986, MNRAS, 219, 575
de Vaucouleurs G., de Vaucouleurs A., Corwin H. G., Buta R. J., Paturel G., Fouqué P., 1992, Third Reference Catalogue of Bright Galaxies. Springer, New York
Disney M. J., Wall J. V., 1977, MNRAS, 179, 235
Ekers R. D., Ekers J. A., 1973, A&A, 24, 247
Ekers R. D., Fanti R., Miley G. K., 1983, A&A, 120, 297
Ekers R. D. et al., 1989, MNRAS, 236, 737
Fabbiano G., Miller L., Trinchieri G., Longair M., Elvis M., 1984, ApJ, 277, 115
Fabbiano G., Klein U., Trinchieri G., Wielebinski R., 1987, ApJ, 312, 111
Fabbiano G., Gioia I. M., Trinchieri G., 1989, ApJ, 347, 127
Feigelson E. D., Nelson P. I., 1985, ApJ, 293, 192
Ghisellini G., Celotti A., George I. M., Fabian A. C., 1992, MNRAS, 258, 776
Giovannini G., 1985, in Dyson J. E., ed., Active Galactic Nuclei. Manchester Univ. Press, Manchester, p. 93
Goss W. M., McAdam W. B., Wellington K. J., Ekers R. D., 1987, MNRAS, 226, 979
Hargrave P. J., 1974, MNRAS, 168, 491
Haynes M., Sramek R. A., 1975, AJ, 80, 673
Heeschen D. S., 1970, AJ, 75, 523
Hummel E., Kotanyi C., 1982, A&A, 106, 183
Impey C. D., Wynn-Williams C. G., Becklin E. E., 1986, ApJ, 309, 572
Isobe T., Feigelson E. D., Nelson P. I., 1986, ApJ, 306, 490
Jones D. L., Wrobel J. M., Shaffer D. B., 1984, ApJ, 276, 480
Kellermann K. I., Pauliny-Toth I. I. K., 1969, ApJ, 155, L71
Kellermann K. I., Pauliny-Toth I. I. K., 1981, ARA&A, 19, 373
LaValley M. P., Isobe T., Feigelson E. D., 1992, BAAS, 24, 839
Lindblad P. O., Jörsäter S., Sandqvist A., 1985, A&A, 144, 496
Meier D. L. et al., 1993, in Davis R. J., Booth R. S., eds, Sub-Arcsecond Radio Astronomy. Cambridge Univ. Press, Cambridge, p. 201
Norris R. P., Kesteven M. J., Wellington K. J., Batty M. J., 1988, ApJS, 67, 85
Norris R. P., Allen D. A., Sramek R. A., Kesteven M. J., Troup E. R., 1990, ApJ, 359, 291
O'Dea C. P., Barvainis R., Challis P. M., 1988, AJ, 96, 435
Orr M. J. L., Browne I. W. A., 1982, MNRAS, 200, 1067
Phillips M. M., Jenkins C. R., Dopita M. A., Sadler E. M., Binette L., 1986, AJ, 91, 1062

Preston R. A., Morabito D. D., Williams J. G., Faulkner J., Jauncey D. L., Nicolson G. D., 1985, AJ, 90, 1599
Readhead A. C. S., Pearson T. J., Barthel P. D., 1988, in Reid M. J., Moran J. M., eds, Proc. IAU Symp. 129, The Impact of VLBI on Astrophysics and Geophysics. Kluwer, Dordrecht, p. 65
Reynolds J. E., Harnett J. I., 1983, Proc. Astron. Soc. Aust., 5, 235
Sadler E. M., 1984a, AJ, 89, 23
Sadler E. M., 1984b, AJ, 89, 34
Sadler E. M., 1984c, AJ, 89, 53
Sadler E. M., Jenkins C. R., Kotanyi C. G., 1989, MNRAS, 240, 591
Scheuer P. A. G., Readhead A. C. S., 1979, Nat, 277, 182
Schmidt M., 1968, ApJ, 151, 393
Schmitt J. H. M. M., 1985, ApJ, 293, 178
Seaquist E. R., Bell M. B., 1977, A&A, 60, L1
Shaver P. A., Churchwell E., Rots A. H., 1977, A&A, 55, 435
Shimmins A. J., Bolton J. G., 1972, Aust. J. Phys. Astrophys. Suppl., 23, 1
Slee O. B., White G. L., Reynolds J. E., Caganoff S., 1990, Astrophys. Lett. Commun., 27, 361
Ulrich M.-H., Meuer D. L., 1984, AJ, 89, 203
Ulvestad J. S., Wilson A. S., 1983, ApJ, 264, L7
Ulvestad J. S., Wilson A. S., 1984, ApJ, 285, 439
van Breugel W. J. M., Schilizzi R. T., Hummel E., Kapahi V. K., 1981, A&A, 96, 310
van den Bergh S., 1989, PASP, 101, 1072
Wall J. V., Schilizzi R. T., 1979, MNRAS, 189, 593
Whiteoak J. B., 1970, Astrophys. Lett., 5, 29
Wrobel J. M., Heeschen D. S., 1984, ApJ, 287, 41
Wrobel J. M., Heeschen D. S., 1991, AJ, 101, 148